

# Manifestations of chaos in billiards: the role of mixed curvature

Pranaya Pratik Das<sup>1,\*</sup>, Tanmayee Patra<sup>1,†</sup> and Biplab Ganguli<sup>1,‡</sup>

<sup>1</sup>*Department of Physics and Astronomy, National Institute of Technology Rourkela, Odisha, India-769008*

(Dated: May 5, 2025)

The boundary of a billiard system plays a crucial role in shaping its dynamics, which may be integrable, mixed, or fully chaotic. When a boundary has varying curvature, it offers a unique setting to study the relation between classical chaos and quantum behaviour. In this study, we introduce two geometrically distinct billiards: a bean-shaped boundary and a peanut-shaped variant of Cassini ovals. These systems incorporate both focusing and defocusing walls with no neutral segments. Our study reveals a strong correlation between classical and quantum dynamics. Our analysis of billiard flow diagrams confirms sensitivity to *initial conditions*(ICs)—a defining feature of chaos. Poincaré maps further show the phase space intricately woven with regions of chaotic motion and stability islands. Moving to the quantum domain, we employ nearest-neighbour spacing distribution and level spacing ratio as statistical measures to characterise chaos. Early time saturation in spectral complexity also supports an ergodic hierarchy in these systems. We observe a striking quantum phenomenon, i.e. eigenfunction scarring. This work bridges geometric boundary effects, classical hyperbolicity, and quantum ergodicity, offering a framework to engineer chaos in confined systems.

**Keywords:** Chaos, Billiards, Billiard flow, Poincaré section, Scars, Rényi entropy, RMT, GUE, Level spacing distribution, Spectral complexity, Quantum chaos

## I. INTRODUCTION

“ Things in motion sooner catch the eye than what not stirs.”

—William Shakespeare, *Troilus and Cressida*

This idea resonates not only in the literature but also in the study of dynamical systems. The exploration of nonlinear dynamics and chaos within Hamiltonian systems offers a multitude of untapped territories and fascinating subjects in both classical and quantum mechanics. Given that quantum mechanics represents a more fundamental perspective of the natural world, it is of utmost importance to study the properties of quantum systems with chaotic classical counterparts[1–3]. There are two classifications for chaotic systems in physics. Dissipative systems, where friction is present, and conservative systems, where energy remains constant throughout the motion. We will only focus on the latter situation here. In this scenario, billiard systems provide significant advantage because of their spatial confinement, which leads to specular (= mirrorlike) reflections<sup>1</sup> [4–8], as illustrated in Fig.(1(a)). Without having to deal with the challenges of integrating the equations of motion to determine its Poincaré map, billiards capture all the complexity of Hamiltonian systems, from integrability to chaotic motion.

In a billiard problem, a point particle moves freely without friction in a two-dimensional enclosed domain  $\Omega \in \mathbb{R}^2$ . Between the elastic collisions at the boundary  $\mathcal{U}$  ( $= d\Omega$ ), the particle travels in straight lines with constant velocity[9, 10]. The billiards with static boundaries can be classified into, at least, three types: (i) integrable billiards (e.g. Circular billiard & Elliptical billiard); (ii) ergodic billiards (e.g. Sinai billiard and the Bunimovich stadium) and; (iii) mixed billiards. In the last case, the phase space shows a mixed behaviour with stable islands existing within the chaotic sea. The present work looks at two models that fall into the category of mixed billiards.

Our primary knowledge in this field largely relies on computational (and, more recently, experimental) investigations conducted on specific model systems. To illustrate the dynamics of a billiard, we assume the Hamiltonian ( $H$ ) of a particle of mass  $m$  which travels freely inside the billiard boundary  $\mathcal{U}$  without friction is given by

$$H(\mathbf{p}, \mathbf{x}) = \frac{1}{2m}(\mathbf{p}^2) + V(\mathbf{x}), \quad (1)$$

---

\* [pranayapratik.das@nitrkl.ac.in](mailto:pranayapratik.das@nitrkl.ac.in)

† [tanmayee.patra@nitrkl.ac.in](mailto:tanmayee.patra@nitrkl.ac.in)

‡ [biplabg@nitrkl.ac.in](mailto:biplabg@nitrkl.ac.in)

<sup>1</sup> Specular reflections refer to reflections in which the angle of incidence before the collision is equal to the angle of reflection after the collision. In other words, particle reflects off the boundary with no change in the tangential component of momentum, and instantaneous reversal of the momentum component normal to the boundary.

where

$$V(\mathbf{x}) = \begin{cases} 0 & \text{If } \mathbf{x} \in \Omega, \\ \infty & \text{If } \mathbf{x} \notin \Omega, \end{cases} \quad (2)$$

The nature of this domain  $\Omega$  ensures the reflection dynamics in the billiard. The kinetic energy term in the system's Hamiltonian guarantees that the particle moves in a straight line between collisions, maintaining constant energy throughout its motion. Because of the inherently simplistic structure of this Hamiltonian, the equations that describe the particle's trajectory-known as the Hamilton-Jacobi equations-are equivalent to the geodesic equations on a manifold. This means that the particle follows geodesics<sup>2</sup>, the shortest paths between points in this domain, further emphasising the deterministic yet potentially chaotic nature of the system.

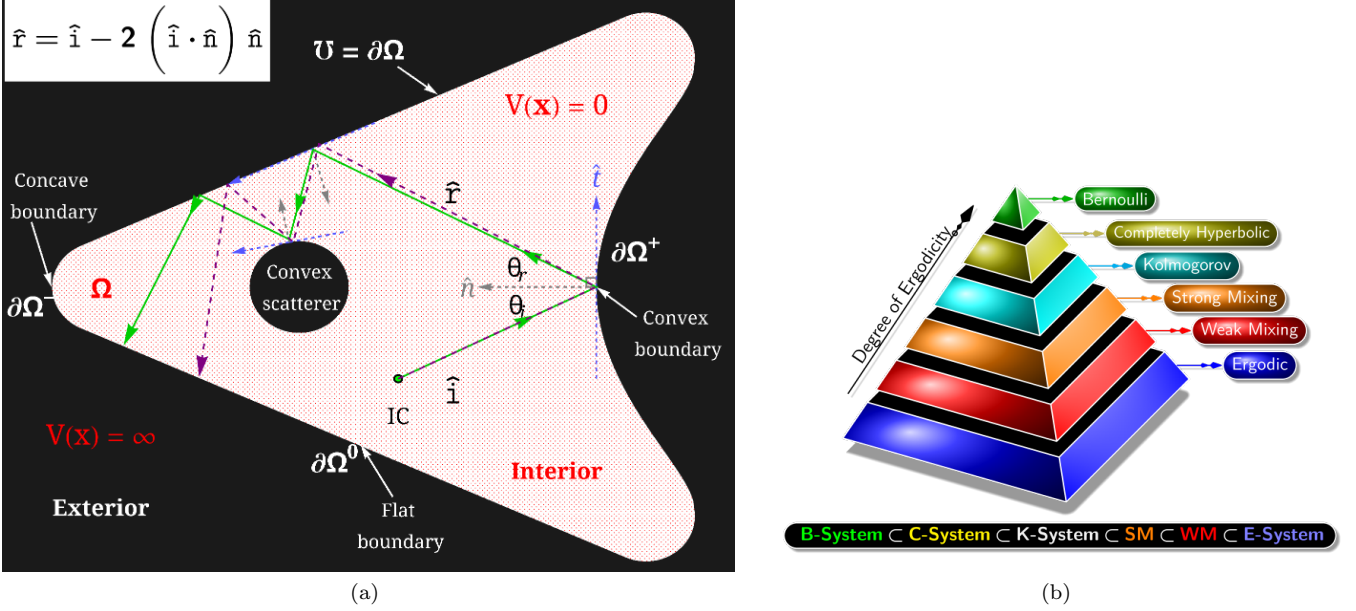


FIG. 1. (a) A schematic representation of two nearby trajectory traced by a particle in a billiard domain ( $\Omega$ ) with boundary ( $U = \partial\Omega$ ). Here  $\hat{r}$ ,  $\hat{i}$  and  $\hat{n}$  are the reflection vector, incident vector, and normal vector at the point of collision, respectively.  $\theta_i$  and  $\theta_r$  are angle of incidence and angle of reflection, respectively and they follow the relation  $\theta_i = \theta_r$  for every collision with the boundary. (b) A pyramid diagram illustrating the Ergodic Hierarchy. Every map that has a higher property, also has the lower properties. The degree of ergodicity is in the order of “increasing chaos”.

For a billiard to display chaotic behaviour in both classical and quantum dynamics, it is essential for it to strictly adhere to the following properties apart from [11, 12]: sensitive to ICs, topologically mixing, ergodic, and positive Lyapunov exponents<sup>3</sup>. The first property ensures that small changes grow rapidly, making prediction difficult. The second condition guarantees the complete mixing of the trajectories over time, ensuring that no regions of the phase space remain isolated. The third ensures that the entire available phase space is filled uniformly. The fourth guarantees divergence of nearby trajectories.

To rigorously characterise their chaotic properties, dynamical systems are often analysed through the lens of the *Ergodic Hierarchy* (EH). The EH is a theoretical framework that categorises chaos into different levels of complexity, with each level including the properties of the levels below it[13]. This hierarchy, illustrated in Fig. (1(b)), provides a scaffold to classify chaos strength, with the Bernoulli systems, at the top, represent the highest degree of ergodicity(stricter stochasticity) and are often associated with the highest degree of chaos[14]. All Bernoulli systems (B-systems) are Complex Hyperbolic systems (C-systems), all C-systems are Kolmogorov systems (K-systems), and so forth. This nesting means that all systems classified within the EH are ergodic; however, the reverse implication does not hold[14–16].

<sup>2</sup> When the particle moves on a non-Euclidean manifold, the Hamiltonian changes to:  $H(\mathbf{p}, \mathbf{x}) = \frac{1}{2m} \mathbf{p}^i \mathbf{p}^j g_{ij}(\mathbf{x}) + V(\mathbf{x})$ , where,  $g_{ij}(\mathbf{x})$  is the metric tensor at point  $\mathbf{x} \in \Omega$ .

<sup>3</sup> In a 2D billiard, out of its four Lyapunov exponents, two must be zero ( $\lambda_2 = \lambda_3 = 0$ ) and the other two are paired in such a way that they sum up to zero, (i.e.  $\lambda_1 = -\lambda_4$ ).

A significant application of the EH framework lies in the study of chaotic billiards, which can be broadly categorised into two types: *scattering billiards* (such as Sinai billiards[17–19] and Periodic Lorentz Gas[20]) and *defocusing billiards* (such as Bunimovich billiards[21, 22], Limaçon Billiard[23], Polygonal Billiards with Rounded Corners[24–27]). A scattering billiard comprises a fixed obstacle (scatterer) with a convex curvature, typically positioned within the billiard boundary as shown in Fig. (1(a)). The reflection from the scattering components is always followed by angle widening of the initially close trajectories (the green and purple trajectories shown in Fig. (1(a))). This eventually leads to chaos. Chaotic behaviour in defocusing billiards results from the defocusing effect caused by the boundary geometry. The defocusing mechanism typically arises when a particle hits a convex boundary[28]. Defocusing mechanism is an alternative to scattering mechanism. In smooth concave billiards, instead of defocusing regions, one finds a focusing regions and hence reflection dynamics becomes regular (e.g., circular and elliptical billiard). Walls with zero curvature are characterised by their straight and flat nature, resulting in reflections that are both predictable and non-chaotic (e.g., triangular, square, hexagonal or other polygonal billiards). Therefore, the nature of reflections in billiards strongly depends on wall geometry, however, these walls do not induce defocusing or focusing effects by themselves.

In this work, we consider the concavity and convexity of the boundary from particle's point of view. In other words, we are addressing the curvature of the wall from inside. A boundary component  $d\Omega$  is classified as focusing (scattering) when it is concave from the inside (outside) of a billiard table. Mathematically, we assume the sign of curvature ( $\kappa$ ) as follows:

$$\kappa = \begin{cases} 0 & \text{If } d\Omega \text{ is flat } (d\Omega^0), \\ +ve & \text{If } d\Omega \text{ is convex } (d\Omega^+), \\ -ve & \text{If } d\Omega \text{ is concave } (d\Omega^-). \end{cases} \quad (3)$$

It is only the boundary of the billiard which determines the dynamical behaviour of the system that can range from integrable, over mixed to completely chaotic[8]. The study of billiards with mixed curvatures, i.e. with boundaries containing both positive and negative curvature components, have received much attention[29–35], because they are the most convenient to realise chaotic dynamics. The interplay between focusing and defocussing effects of concave and convex curvatures, respectively, creates a complex phase space structure that can support a mixture of regular, quasi-periodic, and chaotic trajectories. This simply suggests that there are both chaotic and regular orbits at different parts of the phase space. The alternating focusing and dispersing effects of the mixed curvature amplifies small differences in ICs, leading to chaotic trajectories that explore the phase space more thoroughly. The present work introduces two such chaotic billiards. In contrast to the familiar ones, these include: both focusing and defocusing regions at the boundary, with no neutral components. One of them is bean shaped[36–39], while the other one is peanut shaped, a version of Cassini ovals[40–42]. By altering parameters, we can shape the boundaries of these two billiards to enhance the focusing and defocusing effects. This alteration allows the system to shift from integrability to non-integrability within a single setup.

This tunability is especially significant as it helps us to understand the onset of chaos. Here in this study, we explore the classical and quantum dynamics of these billiards, while our primary focus is on the quantum phenomena. By studying these systems, we aim to investigate how classical chaotic behaviour translates into the quantum regime, particularly observing phenomena such as eigenfunction scarring and spectral complexity. This exploration allows us to bridge the gap between classical chaos and quantum mechanics, offering valuable perspectives on wave behaviour in bounded, irregular spaces where both particle-like and wavelike properties interplay.

The paper is organised as follows. Section (II) introduces billiard models with mixed curvatures (positive and negative), utilising the Bean curve and Cassini curve, detailed in subsections (II A) and (II B), respectively. Next, section (III) presents a classical analysis of billiard dynamics, covering the billiard flow and map in subsections (III A) and (III B), respectively. This section extensively examines the manifestation of classical chaos by analysing trajectories and phase space structures sensitive to ICs which highlight the underlying complex dynamics in these mixed-curvature billiards. Building on this foundation, section (IV) provides a quantum mechanical perspective, demonstrating evidence of eigenfunction scarring within both chaotic billiard models in subsection (IV A) and in the following sub-subsection (??), we use Rényi entropy to quantify these scarings. In subsection (IV B), we numerically assess the nearest level spacing distribution and the level spacing ratio (sub-subsection (IV B 1)) across the four billiard configurations. Subsection (IV C) further explores the spectral complexity of these billiards, where we find strong alignment with the classical results. Finally, section (V) synthesises results obtained and offers a comprehensive discussion and summary of our findings.

## II. MODELS

Dynamical billiards are Hamiltonian systems confined to two spatial dimensions, balancing simplicity and depth. These systems are straightforward to study and visualise, yet they reveal a rich array of complex behaviours, including chaotic dynamics, even when considering a single particle.

In billiard systems, the potential term ensures the particle undergoes specular reflections at the boundaries, while the kinetic term ensures the particle's linear trajectory without altering its energy. Given this straightforward Hamiltonian structure, the particle's equations of motion can be described by the Hamilton–Jacobi equations<sup>4</sup>, representing geodesics<sup>5</sup> on the manifold. The boundary's shape significantly influences the system's dynamics, leading to behaviours that can range from integrable to fully chaotic[28]. This illustrates the broad spectrum of dynamical possibilities in Hamiltonian systems, as exemplified by billiard dynamics [43, 44].

In our model, we have chosen the quartic curve as our base function for the boundary[45]. In algebraic geometry, a quartic plane curve is a fourth-degree curve on a plane. It can be defined by a bivariate quartic equation:

$$Ax^4 + By^4 + Cx^3y + Dx^2y^2 + Exy^3 + Fx^3 + Gy^3 + Hx^2y + Ixy^2 + Jx^2 + Ky^2 + Lxy + Mx + Ny + P = 0 \quad (4)$$

A quartic curve can have a maximum of 4 connected components, 28 bi-tangents, and 3 ordinary double points. In this investigation, two sets of coefficients in the aforementioned equation are analysed for two families of curves, namely bean curves and Cassini ovals, as outlined below. Both Cassini ovals and bean curves are renowned for their symmetrical properties and the diverse range of shapes that can arise from relatively simple mathematical definitions. This makes them highly significant in both theoretical studies and practical applications.

### A. Bean Curves

The Bean curves, discovered by Cundy and Rowlett[36], represent a specific quartic plane curve known for their distinctive bean-like appearance, as illustrated in Fig. (2(a)). With genus<sup>6</sup> zero, it has a singularity at the origin and a triple point.

The curve defining this billiard region is given by,

$$\mathcal{U}_1(x, y, \alpha, \beta) := (x^2 + y^2)^2 - \alpha y(\beta x^2 + \alpha y^2) = 0 \quad (5)$$

Here, with two sets of parameter values we have two different shapes of the billiard as follows

$$\mathcal{U}_1(x, y, \alpha, \beta) = \begin{cases} \text{Circular,} & \text{for } \alpha=2 \text{ \& } \beta=2, \\ \text{Bean,} & \text{for } \alpha=2 \text{ \& } \beta=6 \end{cases} \quad (6)$$

Here, the circular billiard, as we know, has an entirely concave boundary, while the bean-shaped billiard has both concave and convex boundaries.

In contrast to the standard unit bean curve (also known as the egg curve)[37–39], which is located in the first and fourth quadrants, the implicit function denoted as  $\mathcal{U}_1(x, y)$  in Eq. (6), for the bean-shaped billiard defines the boundary in the first and second quadrants.

The Fig. (2(b)) highlights the mathematical evolution of the bean curve and its geometric relationship to a torus. The top row represents the 2D planar depiction of bean curves, along with their corresponding torus sections. It shows the positions of the intersecting plane to generate different curves. In contrast, the bottom row represents the occurrence of these curves in 3D, as toric sections<sup>7</sup> cut by a plane tangent to the torus axis. Each section denotes a different correlation between the parameters  $\alpha$  and  $\beta$ . Under certain conditions between  $\alpha$  and  $\beta$  ( $\alpha < \beta$ ), the bean curve can frequently manifest as a cross-section of the torus. Therefore, the bean curves are toric sections. The details of these curves are beyond the scope of this work, therefore we shall limit ourselves to a rough picture of their forms.

The geometric characteristics of bean curves are presented in Table (I). The shapes of these curves depicted in the Fig. (2(b)) are influenced by the value of  $\beta/\alpha$ . In the case where  $\beta > \alpha$ , the curve takes the form of a singular loop resembling a bean. When  $\alpha = \beta$ , a circle is generated. If  $\alpha > \beta$ , then the curve comprises one loop. However, if the ratio is negative, then the curve consists of three connected loops.

<sup>4</sup> Given the Hamiltonian  $H(\mathbf{p}, \mathbf{x}, t)$ , the Hamilton–Jacobi equation is a first-order, non-linear partial differential equation for Hamilton's principal function  $S : -\frac{\partial S}{\partial t} = H(\frac{\partial S}{\partial t}, \mathbf{x}, t)$

<sup>5</sup> Geodesic equations :  $\frac{d^2 \mathbf{x}^\alpha}{dt^2} = -\Gamma_{\beta\gamma}^\alpha \frac{dx^\beta}{dt} \frac{dx^\gamma}{dt}$  where  $\mathbf{x}^\alpha$  and  $\Gamma_{\beta\gamma}^\alpha$  are the coordinates and the Christoffel symbols, respectively.

<sup>6</sup> The genus of a surface refers to the number of “holes” it contains. For example, a torus has genus 1, while a sphere has genus 0.

<sup>7</sup> Just as a conic section is created by intersecting a cone and a plane, a toric section results from intersecting a torus and a plane.

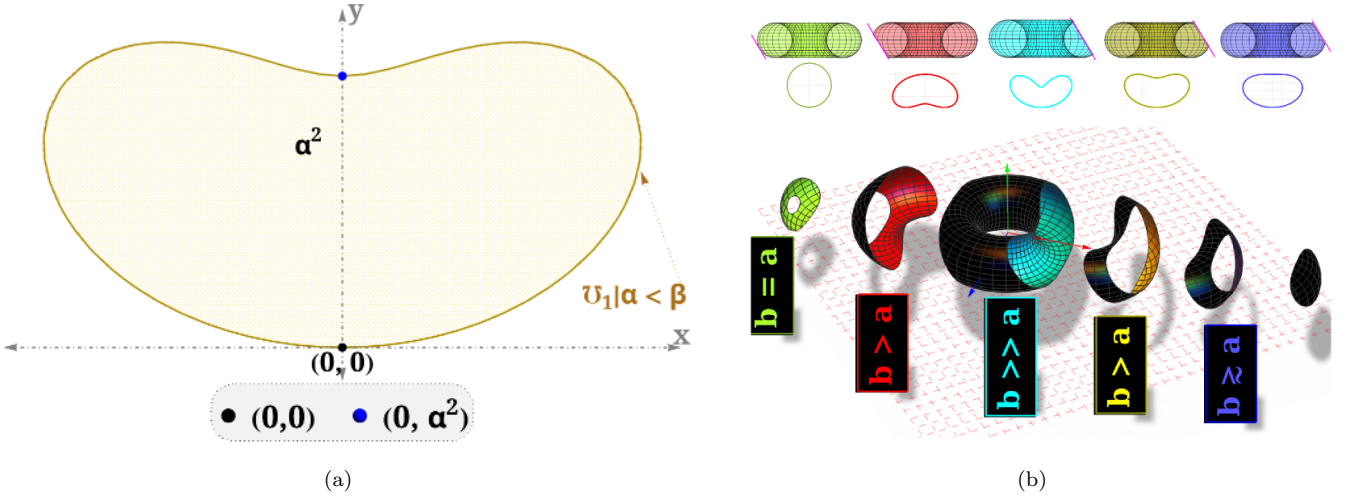


FIG. 2. (a) Bean curve for  $\alpha = 2$  &  $\beta = 6$ . The black, blue and red points are extrema points on the closed curve. (b) Bean curves as planar sections of a torus. The top row features 2D slices of a torus, which take on different shapes from circular to bean-like curves as the parameters  $\alpha$  and  $\beta$  are adjusted. In the bottom row, the torus is shown in 3D, with each toroidal shape representing a different combination of  $\alpha$  and  $\beta$ .

TABLE I. Geometrical Properties Bean and Cassini curves

Properties	Bean curves	Cassini ovals
Intercepts:	$(0, 0), (0, \alpha^2)$	$(\pm\sqrt{a^2 \pm b^2}, 0), (0, \pm\sqrt{b^2 - a^2})$
Extrema:	$(0, \alpha^2), (\pm\sqrt{a^2 \pm b^2}, 0)$	$(0, \pm\sqrt{b^2 - a^2}), (\frac{\pm\sqrt{4a^4 - b^4}}{2a}, \pm\frac{b^2}{2a})$
Symmetries:	$x = 0; (0, 0)$	$x = 0; y = 0; (0, 0)$
Loops:	a single connected loop for $(\pm\alpha, \pm\beta)$ three connected loops for $(\pm\alpha, \mp\beta)$	a single loop if $a < b$ two disconnected loops, if $a \geq b$
Nodes:	$(0, \frac{\alpha^2}{2})$ if $\alpha = \beta$	$(0, 0)$ if $a = b$

## B. Cassini Ovals

The Cassini ovals (also known as Cassini ellipses or Cassinian curves or ovals of Cassini<sup>8</sup>) are quartic curves characterised by the locus of points  $P$  such that the product of the distances from  $P$  to two fixed points,  $F_1$  and  $F_2$  (separated by a distance of  $2a$ ), is  $b^2$ . Mathematically, this is expressed as:

$$|PF_1| \cdot |PF_2| = b^2 \quad (7)$$

where  $b$  is a constant. The implicit function[37, 39, 46],  $U_2(x, y)$ , defining a Cassini oval in Cartesian coordinates, with foci at  $(\pm a, 0)$ , is:

$$U_2(x, y, a, b) := (x^2 + y^2)^2 - 2a^2(x^2 - y^2) + a^4 - b^4 = 0 \quad (8)$$

Here also, we are considering two sets of parameter values that leads two different shapes of the billiard as follows:

$$U_2(x, y, a, b) = \begin{cases} \text{Oval,} & \text{for } a=1 \& b=10, \\ \text{Peanut,} & \text{for } a=1 \& b=\sqrt{1.375} \end{cases} \quad (9)$$

<sup>8</sup> In Italian: Ovali di Cassini, or Ovali cassiniane

Here, the oval<sup>9</sup> billiard has an entirely concave boundary, while the peanut-shaped billiard has both concave and convex boundaries.

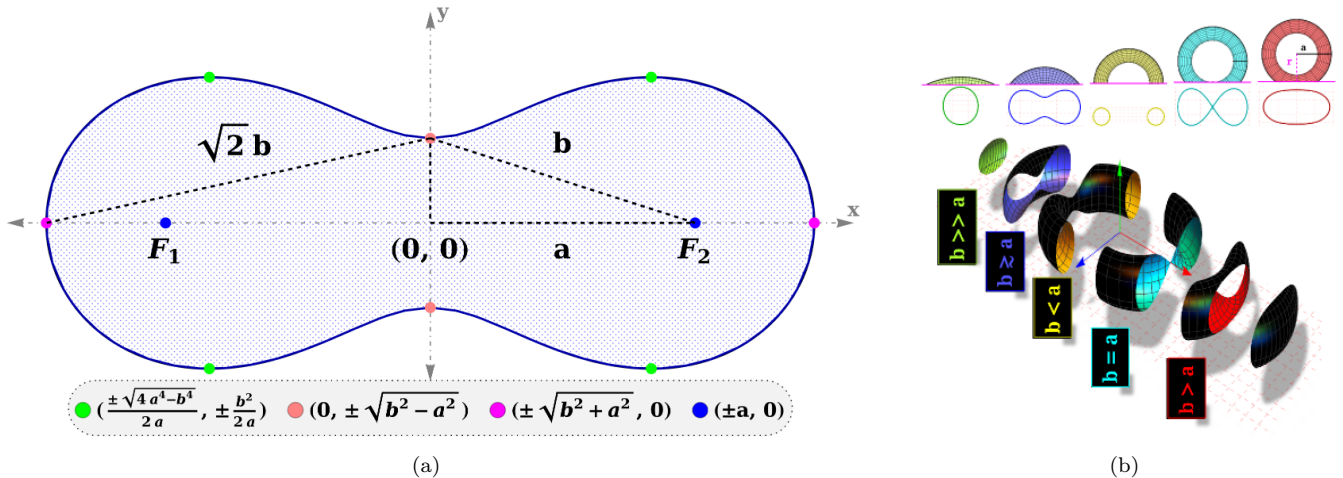


FIG. 3. (a) Cassini oval with two foci ( $F_1$  &  $F_2$ ) at  $(a, 0)$  and  $(-a, 0)$ , respectively. The pink, magenta and green points are extrema points on the closed curve. (b) A family of Cassini Ovals as planar sections of a torus.

The history of Cassini curves dates back to ancient Greek times. However, in scientific history, the French astronomer Giovan Domenico Cassini studied it in 1680 to examine its relation to the motion of the Earth and the Sun[47–51]. Cassini theorised the Sun orbited the Earth, tracing one of these ovals with the Earth at one of the focal points. However, Cassini curves were not suitable for describing planetary motion. In 1694, J. Bernoulli rediscovered them and named them lemniscate in in *Acta Eruditorum*[52]. This rediscovery was important for understanding elliptic integrals and functions. A Cassini oval is an extension of Bernoulli's lemniscate and the ellipse.

Cassini ovals are versatile, finding use in various fields like analytical geometry, nuclear physics, diverse industrial applications, and military systems: various radar and sonar systems use their geometrical properties[53–55]. The blood cells have kitting a biconcave shape similar to Cassini ovals.

The geometrical properties of Cassini ovals are presented in Table (I). The shape of these curves depends on  $b/a$ . When  $a < b$ , the curve has a single loop and resembles an oval or a peanut shape. When  $a = b$ , the curve becomes a lemniscate. When  $a > b$ , the curve has two disconnected loops. Cassini ovals are anallagmatic curves, meaning they are invariant under inversion.

Cassini's ovals are the cross-sections of a circular torus (of radius  $a$ ) cut by a plane parallel to its axis. Let  $r$  represent the distance of the plane from the centre of the torus hole and observe the intersection of this plane with the torus as  $r$  changes. The resulting cross-sectional curves are Cassini ovals, with a lemniscate occurring at  $r = \frac{a}{2}$ . Cassini ovals, as a result, are toric sections. Around 150 BC, the Greek mathematician Perseus studied the sections of a torus, which are now known as the spiroc sections of Perseus [51, 56, 57]. The details of these curves are beyond the scope of this work. Therefore, we shall limit ourselves to a rough picture of their forms[58] as shown in Fig. (3(b)).

Having defined the geometry of the bean and peanut billiards, we now turn to their classical dynamics.

### III. CLASSICAL ANALYSIS

Classical chaos is a phenomenon in nature where deterministic systems display unpredictable behaviour because of sensitivity to ICs[59–61]. A notable example of such chaotic systems can be found in physical and mathematical billiards, which are classified as Hamiltonian systems. And in Hamiltonian systems, there is a natural invariant measure, so the “volume” in phase space is preserved<sup>10</sup>.

Here, rather than constantly monitoring the ball's position and velocity on the frictionless surface, we analyse the measure-preserving billiard map<sup>11</sup>. This map reduces the phase space to a simpler form, focusing only on the boundary

<sup>9</sup> It is an ellipse with eccentricity = 0.14072. Here, in the context of Cassini ovals, we are colloquially referring to this mildly elliptic boundary as an oval.

<sup>10</sup> This property is known as Liouville's theorem, which states that the phase space density of an ensemble of trajectories remains constant as the system evolves.

<sup>11</sup> A billiard map is a discrete-time map that captures the state of the system immediately after each reflection off the boundary.

of the billiard and the angles of reflection. Despite this reduction, the essential dynamics of the system remain intact, allowing for a more straightforward yet still profound analysis of the chaotic nature of such Hamiltonian systems[62].

To begin, let  $\Omega$  be a bounded, closed domain in the plane, where  $\mathcal{U}$  is the boundary of  $\Omega$ , so  $\mathcal{U} = \partial\Omega$ . Orbits of motion are line segments in  $\Omega$  with endpoints on  $\mathcal{U}$ , and adjacent line segments meet on  $\mathcal{U}$ . Motion is always considered with constant velocity in line segments, and collisions with  $\mathcal{U}$  are specular (elastic)[63].

We are now ready to define the concept of a dynamical billiard. Consider a continuous curve  $\mathbf{x}(t)$ ,  $t \in [0, \infty)$ , in  $\Omega$  with the following properties

1. *Boundary Conditions* : The initial condition  $\mathbf{x}(0) \in \Omega$ . This means the particle remains within the domain throughout its motion.
2. *Piecewise Linear* :  $\forall t > 0$ ,  $\mathbf{x}$  consists of linear segments where each segment has its endpoints on  $\mathcal{U}$ . This means that between collisions with the boundary of  $\Omega$ , the trajectory is linear.
3. *Specular Reflection* :  $\forall t > 0$ , the law of reflection holds good, i.e.  $\theta_i = \theta_r$ .
4. *Continuity and Smoothness* :  $x(t)$  is continuous and smooth within  $\partial\Omega (= \mathcal{U})$   $\forall t \in [0, \infty)$ , except at the points of reflection where,  $x(t) \in \partial\Omega$ .

Any trajectory  $\mathbf{x}$  that satisfies the aforementioned properties is termed as a “billiard trajectory”. The collection of all such trajectories forms the dynamical billiard for the region  $\Omega$ . Each billiard trajectory is characterised by a sequence of points that uniquely determine its path. These trajectories comprise linear segments between collisions with the boundary.

In classical mechanics, the motion of a particle within a chaotic billiard is governed entirely by its ICs—its initial position, direction, and speed. Although this determinism might suggest predictability, the path of the particle still appears random because of the irregular nature of the billiard’s boundaries. The evolution of the system can be described through a billiard flow and/or a billiard map. The former refers to the particle’s continuous motion, while the latter presents a discrete-time rendition, focusing on the particle’s state at each collision with the billiard boundary. However, billiard flow is not smooth or differentiable, as each collision with the boundary  $\mathcal{U}$  introduces sudden, discontinuous changes in the particle’s direction. These abrupt shifts highlight the system’s inherent chaotic nature, where the tiniest variations in ICs lead to dramatically different trajectories.

While billiard flow diagrams reveal chaotic trajectories in real space, a more rigorous diagnostic of chaos lies in the phase-space structure. In the following subsection, we employ Poincaré maps to quantify the interplay between regular and chaotic motion.

### A. Billiard flow

The motion of a particle within the billiard is governed by a billiard flow, which characterises the sequence of reflections off the boundary. This flow provides a complete description of the particle’s trajectory by specifying how each reflection leads to the next. The concept of the billiard flow is inspired by an optical analogy, where the phase space is viewed as a space of possible states, and the reflections represent transitions between these states. The motion is confined to invariant tori in integrable systems, while in ergodic systems, the entire energy surface is evenly filled[64]. Through this optical perspective, the billiard flow captures the essential dynamics of the system, offering a comprehensive understanding of the particle’s motion as it interacts with the boundary of the billiard.

Let  $\mathbf{x} \in \Omega$  denote the position of the moving particle and  $\mathbf{v} \in \mathbb{R}^2$  its velocity vector. Of course,  $\mathbf{x} = \mathbf{x}(t)$  and  $\mathbf{v} = \mathbf{v}(t)$  are functions of time  $t \in \mathbb{R}$ . The particle moves with constant velocity between collisions and in between collisions, its motion follows straight lines, so

$$\mathbf{x}(t) = \mathbf{x}_0 + \mathbf{v}(t - t_0) \quad (10)$$

where  $\mathbf{x}_0$  is the initial position, and  $t_0$  is the initial time. Let  $\mathbf{n}$  be the unit normal vector at the point of collision with the billiard wall. If  $\mathbf{v}_{in}$  refers to the pre-collisional velocity, then the post-collisional  $\mathbf{v}_{out}$  is given by,

$$\mathbf{v}_{out} = \mathbf{v}_{in} - 2(\mathbf{v}_{in} \cdot \mathbf{n}) \cdot \mathbf{n} \quad (11)$$

This reflection law ensures the particle’s speed remains constant, but its direction changes depending on the geometry of the boundary. A collision is said to be regular if the vector  $\mathbf{v}_{out}$  is not tangent to  $\partial\Omega$  (i.e  $\mathbf{v}_{in} \neq \mathbf{v}_{out}$ ). However, if  $\mathbf{v}_{out}$  is tangent to  $\partial\Omega$  at the point of collision, then  $\mathbf{v}_{in} = \mathbf{v}_{out}$ , and such a collision is said to be grazing or tangential. Grazing collisions are possible only on convex walls[8] where  $\kappa > 0$ .

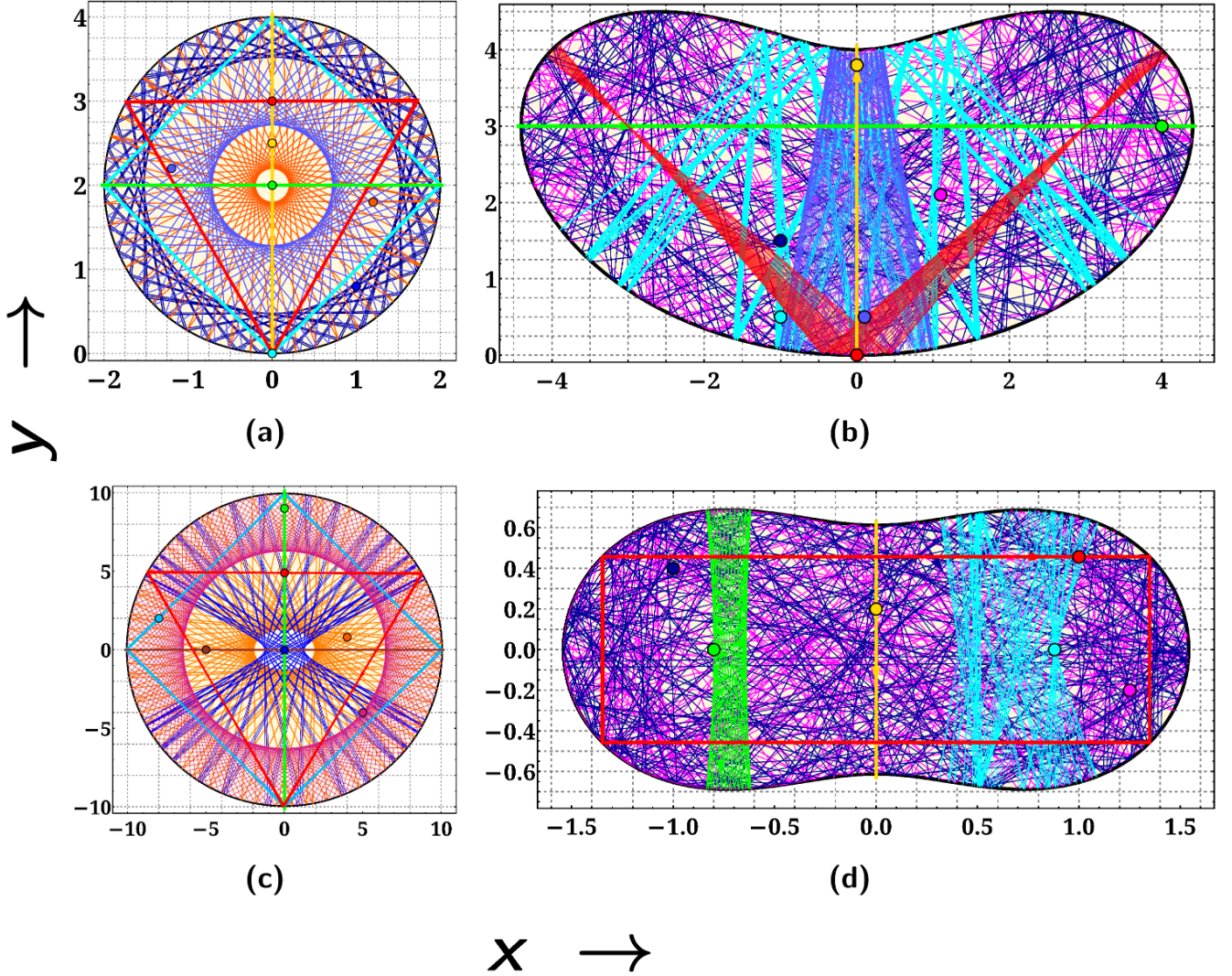


FIG. 4. Billiard flow diagrams representing real space trajectories (periodic, quasi-periodic and chaotic) for (a) Circular, (b) Bean, (c) Oval, and (d) Peanut billiards for different ICs. Typical regular and chaotic trajectories are shown in position space for different ICs. Here, the colourful dots represent different ICs. With circular and oval-shaped billiards, the reflection trajectories are predictable, periodic, or quasi-periodic. Within the boundaries of a circular billiard, every concentric circle acts as a caustic. Conversely, within the oval-shaped billiard, all confocal ellipses, and confocal hyperboloids are caustics. Chaotic trajectories are the norm for bean and peanut-shaped billiards, with only a few specific ICs resulting in periodic outcomes.

Within a regular billiard boundary, and considering classical dynamics, a particle's movement is predictable and periodic. In contrast, a particle in a chaotic billiard follows a random, non-repeating path, though its motion is deterministic. Each bounce off the irregular walls redirects the particle in a way that makes its future path highly sensitive to ICs, resulting in an unpredictable, chaotic motion. Notably, chaotic billiards show both hyperbolicity, meaning nearby trajectories separate exponentially, and ergodicity, meaning a typical trajectory uniformly fills the available space.

The Fig. (4) represents dynamical behaviour on the Bean curves and Cassini curves, following Eq. (6 & 9). Each colour corresponds to a unique IC and the above mentioned figures show how ICs can greatly impact these behaviours. In both regular and chaotic billiards, certain ICs (regions) give rise to periodic orbits, such as orbits of period-two, period-four etc.

In circular and oval billiards, shown in Fig. (4(a) & 4(c)) respectively, the reflections for different ICs result in predictable, periodic, or quasi-periodic trajectories. A particle moving across a circle's diameter has its velocity

reversed upon each collision, resulting in continuous back-and-forth motion along the same diameter, creating a period-two oscillation. Here, the periodicity refers to the number of reflections[14, 65]. Other examples of periodic motion are shown in Fig. (4(a), where the particle traverses the sides of some regular polygons, forming, period-three triangle, and period-four square etc. To be specific, depending on the choice of ICs, concentric circular caustics<sup>12</sup> are formed inside the boundary of the circular billiard. Unlike circular billiard, there exist two foci in the Oval billiard. Here, for each outer trajectory, there is an ellipse with foci at  $F_1$  and  $F_2$ . This ellipse is tangent to each link of that trajectory. Similarly, for each inner trajectory, there is a hyperbola with foci  $F_1$  and  $F_2$ . This hyperbola is also tangent to each link of that trajectory. In conclusion, outer trajectories produce elliptic caustics, while inner trajectories result in hyperbolic caustics.

In Fig. (4(b) & 4(d)), for the bean-shaped and peanut-shaped billiards, we find both regular and chaotic trajectories. By selecting the appropriate ICs, we can identify subregions within these boundaries where trajectories are constrained to specific areas, resulting in periodic or quasi-periodic trajectories. Any other ICs outside these subregions cause trajectories to become non-periodic, filling the space erratically. These results stem from the hyperbolic and ergodic features of chaotic billiards. Unlike regular billiards, single particle dynamics does not produce any caustics here.

Now, let us consider multiple ICs simultaneously. Here, we are considering two sets of ICs[66, 67]: firstly, we are considering all the particles at different  $y$  positions moving parallel to each other and secondly; we fix the  $(x, y)$  position and vary the momentum. As an advantage, this approach yields an envelope of converging trajectories post each reflections from a concave boundary. These trajectories, before diverging, form a denser, high-intensity geometric pattern[68, 69]. In contrast, multiple reflections are involved in producing a caustic using a single IC.

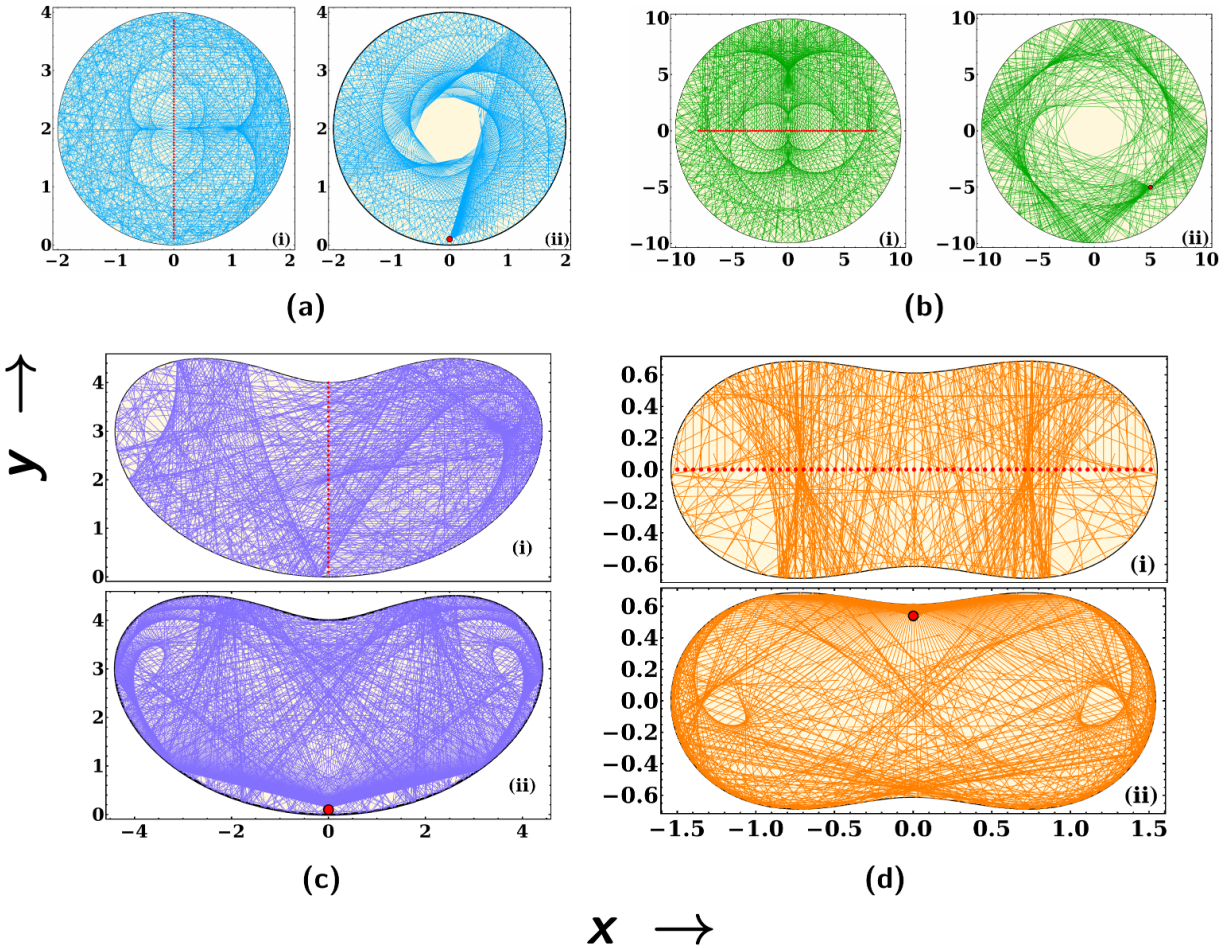


FIG. 5. Caustics produced in (a) Circular, (b) Oval, (c) Bean and (d) Peanut billiards. The red dot(s) represents the IC(s).

<sup>12</sup> Caustics: For a billiard curve ( $\Omega$ ), a curve  $\Gamma$  ( $\subset \Omega$ ) is a caustic, if a ray, once tangent  $\Gamma$ , remains tangent to it after each reflection. The word “caustic” derives from the ancient Greek word *καυστικός* (kaustikos), which translates to “burning”. A caustic curve or surface is the envelope of light rays, creating regions of concentrated light. These curves would look like bright patterns, reminiscent of the shimmering light at the bottom of a pool, and would feel “very hot” if LASER were used.

Fig. (5) shows different intensity patterns in the billiards for the above-mentioned two sets of ICs. For circular and oval billiards (Fig. (5 (a-i)) & 5 (b-i))), because of their smooth concave boundary, the parallel ICs produce cusp-caustics. While ICs for fixed position and varying momenta produce almost indistinguishable patterns (folds and cusps) in both these billiards as shown in Fig. (5 (a-ii)) & 5 (b-ii)). These well organised and reparative patterns correspond to stable structures or constant boundary reflecting integrability of the system[70]. When these boundaries include convex portions, the previously produced repetitive patterns dissolve into more complex non-repetitive patterns. Fig. (5(c) & 5(d)) show various such patterns for bean-shaped and peanut-shaped billiards, respectively. In both these billiards, concave boundary produces converging trajectories leading to cusp like caustics, while the particles bouncing from both concave and convex boundaries produce smoothly varying, broadened and less intense patterns.

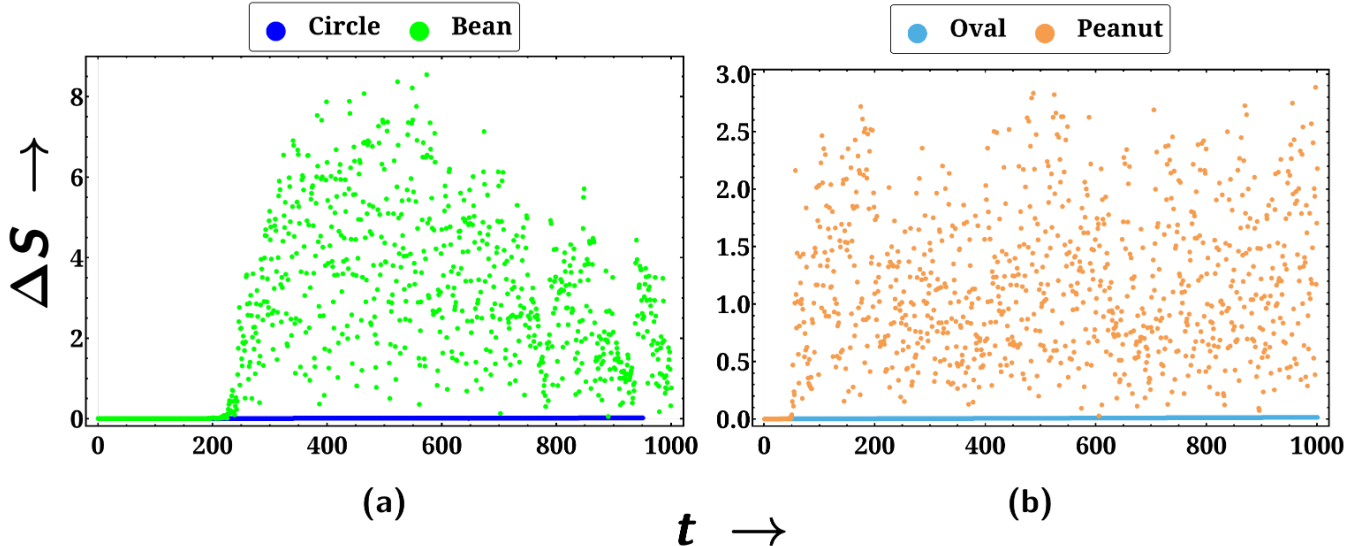


FIG. 6. Measure of divergence ( $\Delta S$ ) vs  $t$  for (a) the bean curve billiards and (b) Cassini oval billiards. The inset graphs shows the linear growth rate for regular billiards namely, circular and oval. On the other hand, chaotic billiards (bean and peanut) have trajectories that rapidly diverge. Here,  $\Delta S$  swiftly attains its maximum—the greatest distance between any two boundary points.

To analyse the divergence of nearby trajectories in different dynamical systems, we consider two sets of initial conditions (ICs):  $(x(0), y(0), p_x(0), p_y(0))$  and  $(x'(0), y'(0), p'_x(0), p'_y(0))$ . These are evolved over time using the mapping dynamics discussed previously. The prime coordinates are initialised with  $x'(0) \rightarrow x(0) + \delta_0$  and  $y'(0) \rightarrow y(0) + \delta_0$ , whereas,  $p'_x(0) \rightarrow p_x(0)$  and  $p'_y(0) \rightarrow p_y(0)$ . After evolving them for a finite time ( $t = 1000$ ), we measure the distance between them as  $\Delta S = \sqrt{(\Delta x)^2 + (\Delta y)^2}$ . Fig. (6) shows how  $\Delta S$  varies with time for different billiards.

In integrable billiards, such as circular and oval-shaped billiards, nearby trajectories grow linearly or slower over time. This means that the divergence of trajectories is limited and they remain relatively close and predictable. On the other hand, chaotic billiards exhibit rapid divergence of trajectories, resulting in unpredictable and seemingly random motion. In chaotic billiards,  $\Delta S$  can rapidly grow to its maximum value, i.e. the maximum distance between two points on the billiard boundary.

## B. Billiard map

By using the Poincaré surface of section (SOS) method, classical billiard dynamics can be simplified to a two-dimensional discrete mapping. This method utilises the boundary of the billiard table as the SOS to discretize the dynamics. A billiard flow has a natural Poincaré section defined by Birkhoff coordinates[71]. These coordinates are the arc-length position of the  $n^{th}$  bounce along the billiard boundary ( $\partial\Omega$ ), denoted by  $\xi$ , and the tangential component of momentum at the boundary, denoted by  $p_n = |p| \sin(\phi_n)$ . Here,  $\phi_n$  represents the angle between the outgoing trajectory and the normal to the boundary [4, 71–74]. Both the arc length  $\xi$  and the tangential momentum  $p$  are measured counter-clockwise relative to the outward normal. Here, each point in the Poincaré section represents a collision event characterised by the location of the particle on the boundary and the angle of the reflection. Over

time, as the particle bounces around, a collection of points forms the collision space with coordinates  $\phi$  and  $\xi$ , which we call the Poincaré map or the collision map  $\mathcal{P}$ .

When visualised in two dimensions, the Poincaré section takes the form of a cylinder, topologically akin to an annulus. The tangential momentum, denoted by  $p$ , ranges from  $-|p|$  to  $|p|$ . Meanwhile, the coordinate  $\xi$  exhibits cyclic behaviour along every connected section of the boundary  $\partial\Omega$ . Liouville's theorem guarantees the preservation of volume in the full phase space. And given the conservation of kinetic energy in elastic collisions, we conventionally assign the mass and magnitude of momentum for the billiard-ball to  $m = |p| = 1$ . As a result, the Poincaré section condition reduces the dimensionality by one, while energy conservation removes another dimension. Therefore, the map  $\mathcal{P}$  is  $(2D - 2)$ -dimensional. Due to the straight-line motion within the billiard, using the boundary to define a Poincaré section is practical. Mathematically,

$$\mathcal{P} := (\xi, p) \mid \xi \in [0, |\partial\Omega|], p \in [-1, 1] \quad (12)$$

The dynamics from the  $n^{th}$  collision to the  $(n + 1)^{th}$  collision is given by

$$\mathcal{P} : (\xi_n, \sin(\phi_n)) \mapsto (\xi_{n+1}, \sin(\phi_{n+1})) \quad (13)$$

where,  $\xi \in [0, L]$ <sup>13</sup> and  $\psi \in [0, \pi]$ , which is the angle between the particle's velocity vector and the normal vector at the collision point. Note that, The collision map  $\mathcal{P}$  also admits an involution, i.e.  $(\xi, p) \mapsto (\xi, -p)$ .

Regular orbits on a Poincaré section appear orderly and confined. They appear as points or closed curves, indicating periodic or quasi-periodic motion. Chaotic trajectories, on the other hand, scatter irregularly and fill the available phase space in a disorder manner. The subregions dominated by quasi-periodic orbits are often surrounded by chaotic regions. This coexistence creates a complex structure in phase space, where stable, regular areas are interwoven with chaotic zones[75].

Billiard Map for our chosen billiard boundaries are shown in Fig. (7) along with a qualitative demonstration of their corresponding billiard flow diagrams. In Fig. (7(a)), for circular billiard the points on the Poincaré section form distinct and repeating patterns, indicating stability and lack of chaos. In Fig. (7(c)), for the oval boundary, the points fall in an organised manner, forming closed loops and smooth curves, indicating periodic or quasi-periodic motion. Trajectories through the foci form an “∞-shaped” closed curve on  $\mathcal{P}$ , separating distinct regions of closed and open curves [8]. All the trajectories tangent to the elliptic caustics form “horizontal waves” on the collision space  $\mathcal{P}$ . The inner trajectories form the closed loops inside the ∞-shape, while all outer trajectories are responsible for the horizontal waves beyond the ∞-shape.

In contrast, for bean-shaped (Fig. 7(b)) and peanut shaped (Fig. 7(d)) billiards, the points scatter more randomly and lack a clear repeating pattern, though they coexist with regions where points form closed loops (islands of stabilities). Here, the Poincaré section shows both well-organised regions (regular) and disorganised areas (chaotic) and the particle can switch between these regions, depending on its position and velocity. Notably, at the edges of these islands of stabilities, fractals structures emerge for both the billiards. The fractals in the Poincaré section encapsulate the essence of chaos.

A particularly intriguing feature observed is that the points in the chaotic sea surrounding the regular islands are not uniformly distributed. In the Bean-shaped billiard, points cluster more densely near either side of the boundary (left and right), while in the peanut-shaped billiard, the chaotic sea has alternating zones of high and low density of points forming patch like structure. This uneven distribution of points is typical of chaotic systems, where some trajectories are favoured more than others due to the underlying geometry of the boundary. The high density regions correspond to areas where there is a temporary confinement or “trapping” of the trajectories, whereas the low-density regions might correspond to zones that are dynamically “repulsive” or less accessible.

#### IV. QUANTUM MECHANICAL ANALYSIS

To develop a more comprehensive understanding of classical chaos, it is essential to investigate it through the lens of quantum mechanics [76]. However, the classical approach is rendered infeasible by the Heisenberg uncertainty principle, which limits our ability to precisely measure both position and momentum simultaneously, forcing us to seek a different approach. In quantum mechanics, the state of a particle is represented by a wavefunction, with the square of its magnitude providing the corresponding probability density. Therefore, quantum chaos research focuses on examining the statistical characteristics of eigenfunctions and energy levels, rather than tracking the system's temporal dynamics.

---

<sup>13</sup>  $L = |\partial\Omega|$  is the total perimeter of  $\partial\Omega$ .

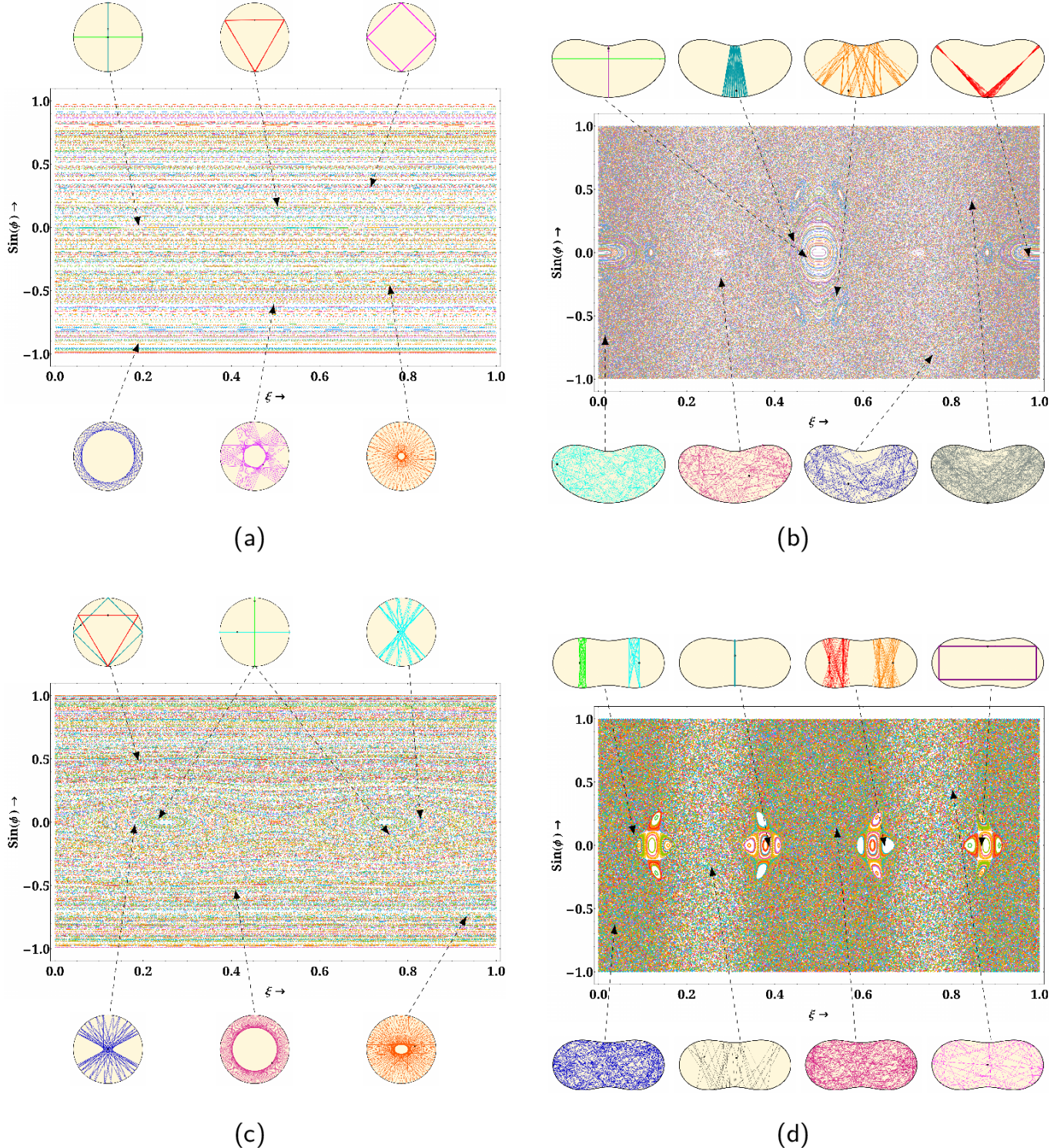


FIG. 7. Poincaré section of (a) Circular Billiard, (b) Bean Billiard, (c) Oval Billiard and (b) Peanut Billiard. In circular and oval billiards, trajectories follow invariant curves in the  $(\xi, \sin(\phi))$  plane, suggesting regular motion. Conversely, bean and peanut-shaped billiards exhibit a mixed phase space in the section, featuring chaotic regions (scattered points), islands of stability, and fractal structures, illustrating the system's diverse dynamics. The surrounding trajectories, displayed in position space, qualitatively indicate the location of the Birkhoff coordinates on the Poincaré section.

The well-known linear Schrödinger equation:

$$\hat{\mathcal{H}}\psi(\mathbf{x}) = \left( \frac{-\hbar^2}{2m} \nabla^2 + V(\mathbf{x}) \right) \psi(\mathbf{x}) = \mathcal{E}\psi(\mathbf{x}) \quad (14)$$

Here, we adopt the units:  $\hbar = k_B = m = 1$ . Since potential inside the billiard is zero ( $V(\mathbf{x}) = 0 \forall \mathbf{x} \in \Omega$ ), this equation reduces to Helmholtz equation:

$$\left( \frac{-1}{2} \nabla^2 \right) \psi(\mathbf{x}) = k^2 \psi(\mathbf{x}), \quad \forall \mathbf{x} \in \Omega \quad (15)$$

with Dirichlet boundary conditions, i.e.  $\psi(\mathbf{x}) = 0 \forall \mathbf{x} \in \partial\Omega$ . Here  $\nabla^2$  denotes the Laplace operator, which reads in two dimensions  $\nabla^2 = (\frac{\partial^2}{\partial x_1^2} + \frac{\partial^2}{\partial x_2^2})$ . Here, the eigenenergy  $\mathcal{E} = k^2$ , where  $k$  is the wave number, and the interpretation of  $\psi$  is that  $\int_{\mathcal{D}} |\psi(\mathbf{x})|^2 d^2\mathbf{x}$  is the probability of finding the particle inside the domain  $\mathcal{D} \subset \Omega$ . In quantum billiards, we find the stationary solutions of the Schrödinger equation by determining the eigenvalues and eigenfunctions of the Helmholtz equation. These eigenfunctions and eigenvalues give us insights into the quantum equivalents of classical chaotic behaviour.

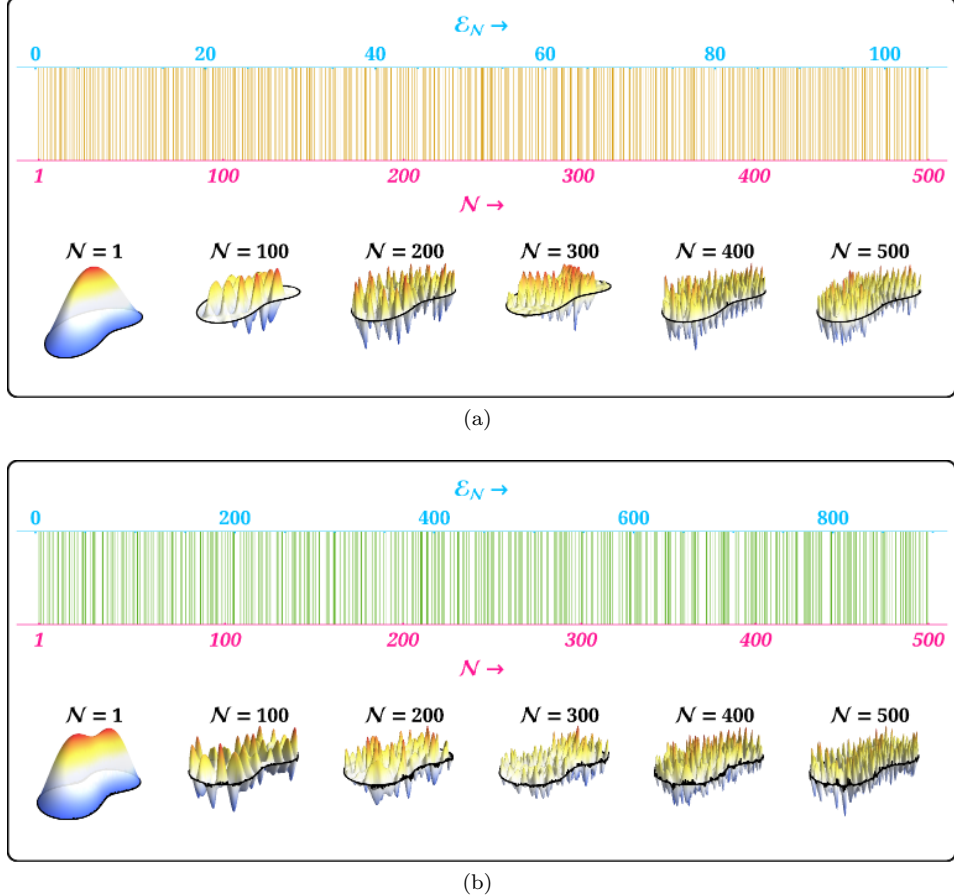


FIG. 8. First 500 eigenvalue spectra for (a) Bean-shaped Billiard and (b) Peanut-shaped Billiard with a few selected eigenstates. In each figure, the upper and lower rows represent spectra of eigenvalue and a few selective eigenstates, respectively.

For certain simple domain, it is possible to solve Eq. (15) analytically. However, numerical techniques such as *Finite Difference Method* (FDM)[77–79], *Finite Element Method* (FEM)[80–83], *Boundary Element Method* (BEM)[84–87], etc. are commonly employed for more complex domains. In this work, we have employed FEM<sup>14</sup> to compute over

<sup>14</sup> FEM, well-suited for irregular domains, subdivides the area into finer elements and approximates the solution with piecewise polynomials, offering higher accuracy.

$4 \times 10^4$  eigenvalues for both the models under consideration. Concerning the numerical implementation this is the most time consuming step<sup>15</sup>. The numerical results for the eigenvalues and eigenfunctions are presented in Fig. (8). Fig. (8(a)) displays the outcomes for the Bean-shaped billiards, while Fig. (8(b)) illustrates the results for the Peanut-shaped billiards.

In Fig.(8(a) & 8(b)), the vertical lines (yellow and green lines) indicate energy eigenvalues  $\mathcal{E}_N$  corresponding to their quantum numbers  $N$ , with  $N$  ranging from 1 to 500. The spacing between the eigenvalues appears small, but non-uniform. This irregularity in spacing provide insights into the nature of the system's behaviour, which will be further explored in the following sections.

Fig.(8(a) & 8(b)) also shows the eigenstates corresponding to different  $N$ . The colour gradient likely represents the amplitude of the eigenfunction (red for high amplitude, blue for low amplitude), with the wavefunction oscillating between positive and negative values. The shapes of these eigenstates directly relate to the potential governing the system, with each eigenstate reflecting the spatial distribution of the probability density for a particle.

### A. Evidence of scarring

In quantum systems, the idea of a precise trajectory fades away, replaced by a landscape of probability where particles can be found. Despite particles not adhering to a solitary, predetermined path, the collective impact of their various potential routes can cause discernible characteristics reminiscent of classical paths. A particularly fascinating phenomenon in this context is that of quantum scars.

From quantum mechanical standpoint, the wave function plays a crucial role in determining how particles behave. Hence, in translating ergodicity to the quantum realm, it is logical to assume that the corresponding wavefunctions ( $\psi_N$ ) of an ergodic system would exhibit the same level of chaos and distribute uniformly throughout the entire energy shell as  $N \rightarrow \infty$  or in the semiclassical limit  $\hbar \rightarrow 0$ . This is the content of *quantum ergodicity theorem*[88–92] and is indeed correct for almost all eigenstates. However, there are exceptions. In quantum chaotic systems, some eigenfunctions show high probability density regions that seem to “favour” certain classical periodic trajectories. Such periodic trajectories are unstable, meaning that even a small deviation from the path would quickly lead to divergence. Nonetheless, in the quantum case, the wave function “remembers” these unstable paths (“slow diverging” or “near marginally stable”), where the probability density is disproportionately high. This concentration of probability density of quantum states along a classical periodic trajectory is called a quantum scar[93–99]. Even though quantum systems typically evolve toward thermal equilibrium, effectively erasing the memory of their ICs[100], scarred states are more likely to stay close to their initial periodic orbits that are not too unstable.

This effect is particularly evident when the trajectories governing the classical system are chaotic. However, this does not happen in the corresponding quantum system. The quantum system retains a memory of its classical IC, even in the infinite time limit, thereby disrupting the ergodic nature of the system. This suggests that the system has an enhanced probability of remaining around its non-periodic, slow diverging trajectories. This lead to a type localisation in the probability density of quantum observables irrespective of periodicity. These localisations are not limited to a single eigenstate. Instead, they affect a wide range of quantum eigenstates and have some structure along any trajectory as long as the rate of divergence is slow. Different names have been proposed by different authors for this kind of localisation: “quantum trails” [101], “quantum birthmark”[102]. In Fig. (10), a visualisation on this account is provided, taking the peanut-shaped billiard as an example. Presented in the left column is a slowly diverging classical trajectory for an IC at two different times: at  $t = 15$ , nearly periodic behaviour and at  $t = 120$ , chaotic behaviour. The accompanying probability density graph (on the right) shows that the eigenstate, with  $E = 1815.56$ , is sharply localised along the classical trajectory at the early time. A few other scars for slow diverging classical trajectories are provided in Appendix-A 2, Fig. (16) for both bean and peanut shaped billiards.

Unlike scars, super-scars[103–108] are more structured and strongly localised that arise not from unstable/stable periodic orbits, but rather from higher symmetry or dynamical constraints in the system. They represent more extensive and stable quantum states that are confined to special regions of phase space (e.g., modes confined to certain shapes or regions of the billiard table). These states are often related to “nongeneric”[94, 109] features of the classical system, such as symmetry or specific boundary conditions, that impose additional constraints on the wavefunctions. In these cases, the classical periodic orbit structure is not known.

It is possible for different eigenstates of a quantum system to exhibit scars associated with classical unstable periodic orbits, while others display super-scars related to the system's symmetries or special constraints. The presence of both types of localisation depends on the system's geometry, symmetries, and dynamical properties, with different

---

<sup>15</sup> The Helmholtz equation (Eq. 15) was solved using the finite element method (FEM) in **Mathematica** 14.0. The domain  $\Omega$  was discretized using a triangular mesh with maximum cell size controlled by the parameter **MaxCellMeasure**.

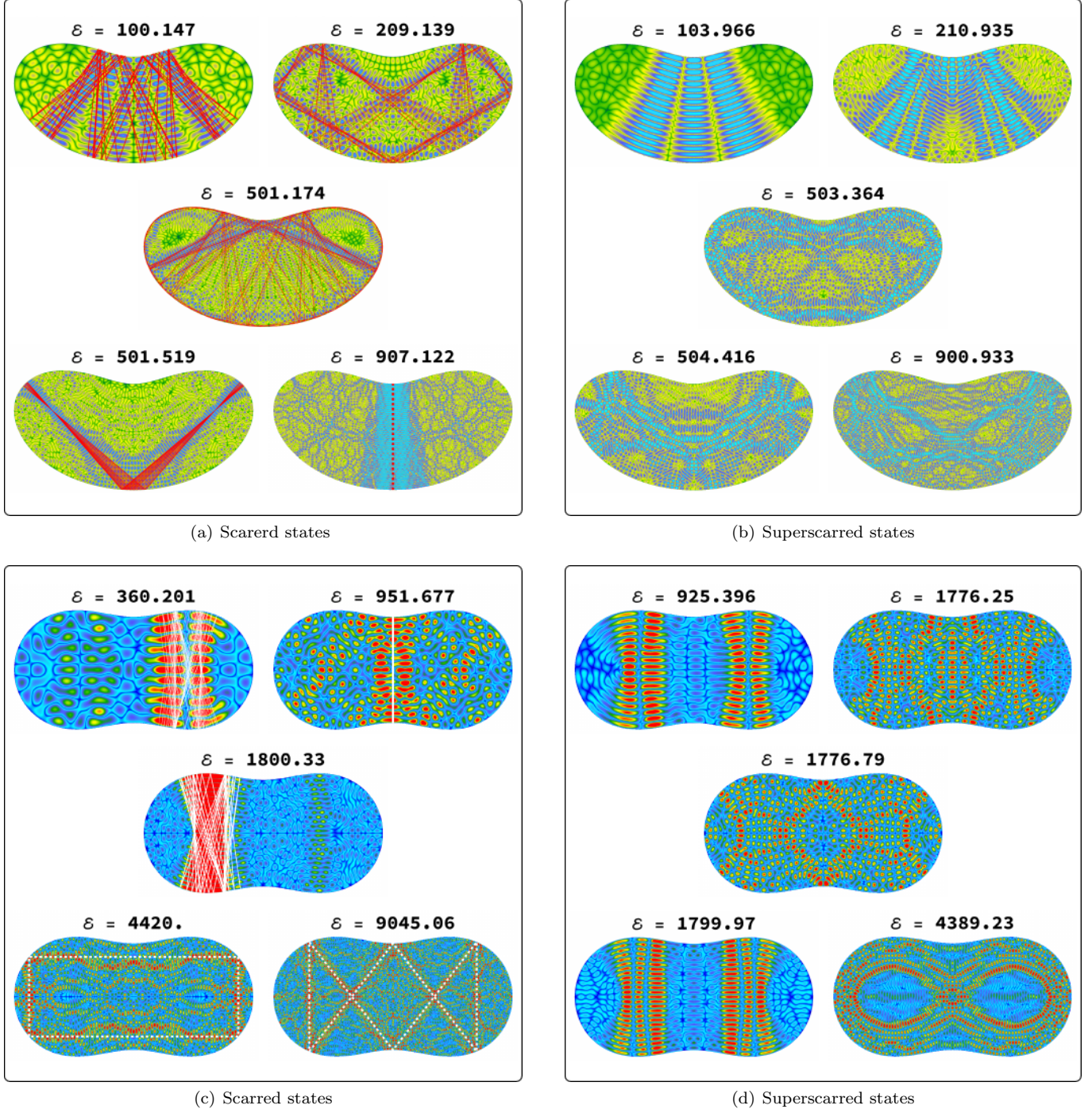


FIG. 9. The probability density distributions for eigenstates are displayed for billiards: (a & b) the Bean-shaped billiard and (c & d) the Peanut-shaped billiard. In both chaotic billiards, some eigenstates (a & c) concentrate along specific isolated, trajectories of the corresponding classical system, highlighted by solid red and white lines. These concentrated patterns, known as quantum scars. In contrast, for the super-scars observed in the Bean and Peanut-shaped billiards (b & d), there is no corresponding classical orbit present.

eigenstates or energy levels reflecting different types of localisation. These form the skeleton of the classical phase space structure[9] and weakly breaks ergodicity, meaning that the system does not explore all possible states equally over long times. Scars serve as vivid illustrations of how quantum mechanics suppresses chaos[10].

The theory of quantum scars has limitations. While it predicts an enhancement of the wavefunction along classical

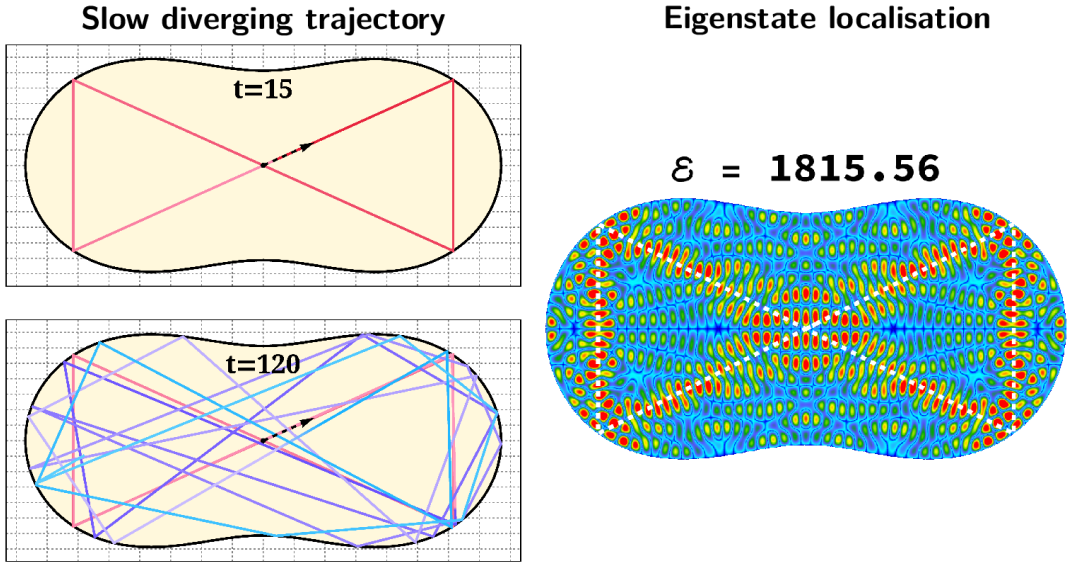


FIG. 10. In the left column, a slow diverging trajectory in the peanut billiard shows almost periodic and chaotic behaviour in the early and late time, respectively. The right column shows a probability density plot producing a scar at energy  $\mathcal{E} = 1815.56$ . It is evident that the quantum systems keep a memory of its classical IC even in the infinite time limit.

paths, it cannot precisely determine which quantum states will exhibit scarring or to what extent. It offers only a general guideline suggesting that some states within specific energy ranges may show scarring, but the precise details remain uncertain. Although the precise origins of quantum scarring remain unclear, one proposed explanation suggests that these scars might reflect integrable or nearly integrable systems. Scars represent non-ergodic states, a concept allowed by quantum ergodicity theorems [111]. This is contrary to the general expectation of ergodic behaviour in chaotic systems, where all accessible states are equally probable. Quantum scars suggest that even in a chaotic system, some quantum states retain a memory of classical periodic orbits.

Fig. (9) shows probability density structures of quantum states in the above mentioned billiard systems, highlighting regions where the density is higher. For the Bean billiard, the energy of the eigenstates can be anywhere between 40 and 910, while for the Peanut billiard, it ranges from 350 to 9056. The overall background represents the typical distribution of the quantum state in a chaotic system, which is usually spread out and somewhat uniform. Scarred regions, Fig. (9(a) & 9(c)), are the areas where the probability density is significantly higher. They appear as dark isolated lines or spots in the diagram, corresponding to the classical periodic orbits (solid red & white lines). On the other hand, in the super-scarred states ( Fig. (9(b) & 9(d))), the probability densities do not align with any classical orbits, indicating a lack of classical periodic orbit influence. In contrast to non-integrable billiards, the eigenfunctions of integrable billiards are confined to specific subregions of the billiard[64], predominantly localized around the caustics[112] found in their corresponding classical systems (see Appendix-A 1, Fig. (15) for more details).

These localised regions act like “mirages” in the quantum landscape, where the eigenfunction gets focused because of the underlying classical dynamics. A comparison of scars across various energy levels reveals that they emerge only for a selected few eigenvalues. The level of scarring associated with specific eigenstates varies significantly from one state to another, although it aligns with a theoretically predicted distribution. This selective nature makes these scars especially intriguing. They form along moderately unstable, relatively short periodic orbits and occasionally exhibit symmetrical distribution based on the geometry. Scars are a concept absent in the realm of classical mechanics.

### B. Level spacing distribution

The *Bohigas-Giannoni-Schmit* (BGS) conjecture, originating from the pioneering work of Bohigas, Giannoni, and Schmit in 1984[113], is a fundamental discovery in the field of quantum chaos. It states that the energy spectra of quantum systems, which exhibit complete classical chaos (governed by autonomous Hamiltonians and ergodic behaviour), display statistical properties that can be described using Gaussian *Random Matrix Theory* (RMT)[111, 114–116] when examined in the semi-classical limit. The “semi-classical eigenfunction hypothesis” suggests that the eigenstates of these systems should primarily concentrate in regions that are explored by generic orbits over

long periods of time[115, 117–119]. Then the random matrix approximation, in conjunction with the energy-time uncertainty principle, allows us to understand the long time dynamics in chaotic systems by analysing the statistics of nearby eigenvalues of the Hamiltonian.

The *Nearest Neighbour Spacing Distributions* (NNSD) serve as a primary indicator of quantum chaos. In this context, we define level spacing as the energy gap between two neighbouring levels in the unfolded spectrum, denoted by  $s_i = \tilde{\mathcal{E}}_{i+1} - \tilde{\mathcal{E}}_i$ . The unfolding procedure<sup>16</sup> ensures that the mean level spacing is normalised to unity. The *level spacing distribution*,  $P(s)$ , takes centre stage, providing degree of level repulsion. A dramatic insight in the field of quantum chaos is summarised by the universality conjectures for  $P(s)$ :

$$P(s) = \begin{cases} e^{-s} & \text{Poissonian,} \\ \frac{\pi s}{2} e^{-\frac{\pi s^2}{4}} & \text{Gauss Orthogonal Ensemble (GOE),} \\ \frac{4s^2}{\pi^2} & \text{Gauss Unitary Ensemble (GUE)} \end{cases} \quad (16)$$

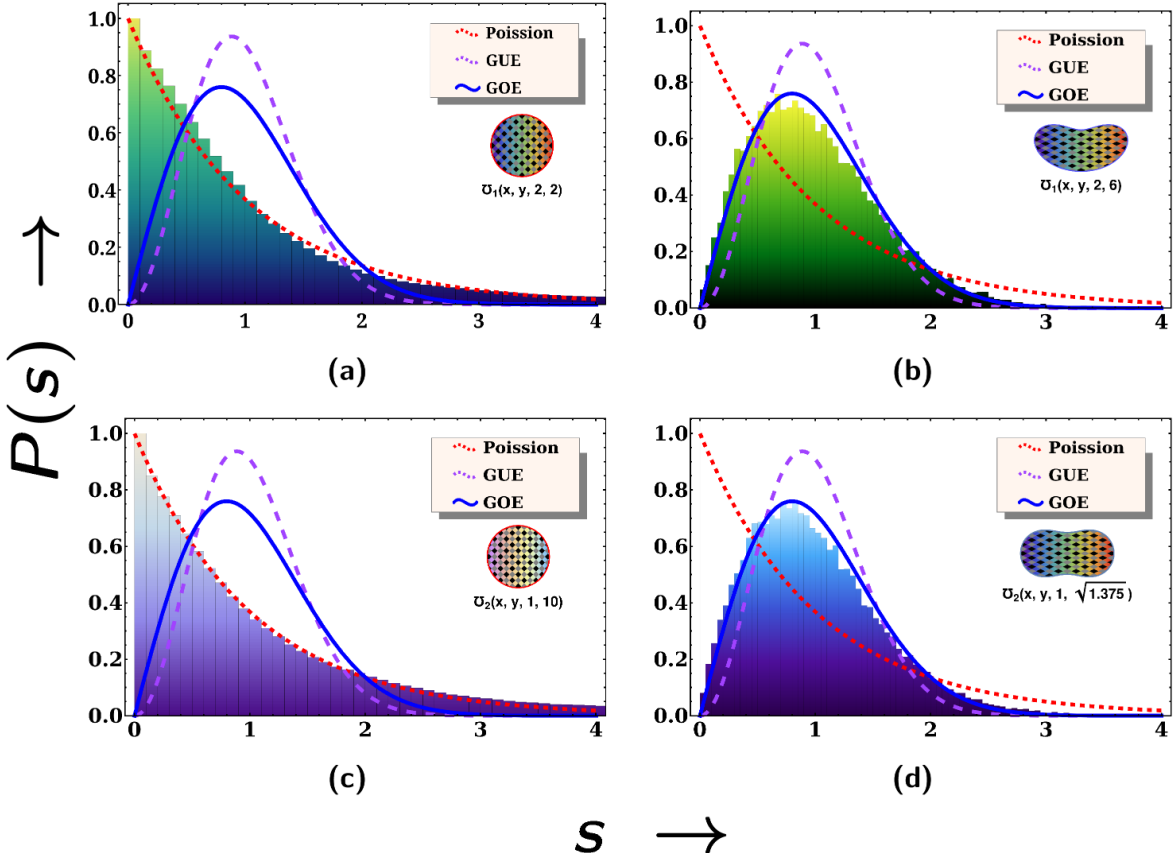


FIG. 11. NNSD for (a) Circle, (b) Bean (c) Oval and (d) Peanut billiards with  $\mathcal{N}$  ranging between  $2 \times 10^4$  to  $4 \times 10^4$ . There is a strong agreement between the observed behaviour and the expected behaviour of a Poissonian random process and the GOE, respectively.

Chaotic systems with time-reversal symmetry show energy level spacing statistics that align with the GOE of RMT. This alignment can be well approximated by the *Wigner-Dyson* (WD) distribution[113, 120]. The WD distribution

<sup>16</sup> Analysing the level spacing distribution involves two key steps: unfolding the eigenvalues and segregating them based on symmetry sectors. Unfolding imposes rescaling the eigenvalues to ensure that the local density of states at the rescaled energies equals 1. In other words, the unfolding procedure guarantees that the mean level spacing is unity. Segregating by subspaces is essential because eigenvalues originating from distinct symmetry sectors lack inherent correlation.

indicates that the eigenvalues are correlated, leading to *level repulsion*[121]. Specifically, the probability  $P(s) \rightarrow 0$  at small and large distances, signifying that energy levels tend to avoid clustering. The graph of this distribution has a peak and then tails off, capturing the repulsion at small distances ( $s \rightarrow 0$ ) and random-like spread at larger distances ( $s \rightarrow \infty$ ). It is noteworthy that the zeros of the Riemann zeta function display a similar distribution[122, 123]. On the other hand, for generic integrable classical systems, Berry, and Tabor [124] conjectured that the level spacing distribution follows Poisson statistics. Here, energy levels are uncorrelated, leading to *level attraction*, where  $P(s) \rightarrow 1$  as  $s \rightarrow 0$ . This shows that small spacings between energy levels are more likely to occur randomly without significant interaction. Thus, investigating the distribution of energy level spacings offers insight into the nature of correlations between levels, with level repulsion dominating in chaotic systems and level attraction prevalent in integrable systems.

The Poisson distribution implies that level crossings are allowed[125]. Whereas, the WD or GOE distribution indicates towards presence of avoided crossings. In essence, the observation of a Poisson or GOE distribution in the level spacing serves as a distinct characteristic of a quantum integrable or chaotic system, respectively. In Fig. (11), the circular and oval-shaped billiards (Figs. (11(a)) and (11(c))) exhibit Poisson distributions, which aligns with their classical nature. This agreement is excellent, as it implies that the energy levels have no correlation. Meanwhile, for the bean and peanut-shaped billiards (Figs. (11(b)) and (11(d))), we observe GOE distributions, confirming their chaotic behaviour.

To verify the convergence of these results, we ran numerical evaluations for  $\mathcal{N} = 2000, 5000, 20000$ , and  $40000$ , yielding consistent results for each of the billiards.

Whenever the agreement of one of the distributions  $P(s)$  with data or numerical calculations is tested, it is helpful to use the cumulative level-spacing distribution[126, 127] given by  $I(s) = \int_0^s P(s')ds'$ . It is independent of binning effects<sup>17</sup>. In other words, it is much smoother and less sensitive to statistical fluctuations (noise) than the raw NLSD, especially for small or moderately sized datasets.

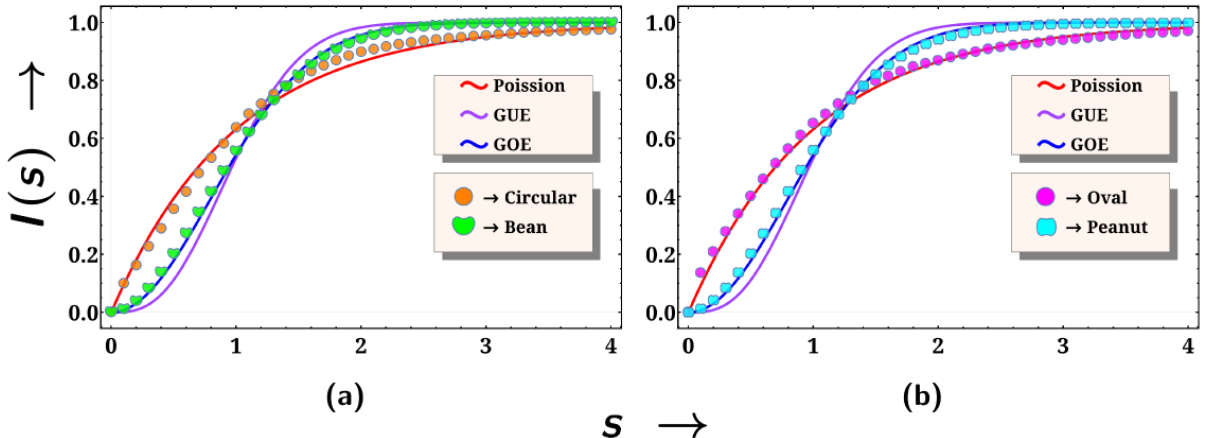


FIG. 12. The cumulative level-spacing distribution  $I(s)$  for the four billiards. Circular and Oval billiard follows Poisson distribution, while Bean and Peanut billiard aligns with GOE. Deviations from these curves signal mixed dynamics or finite-size effects.

Fig. (12) shows the variation of  $I(s)$  for the four billiards. For circular and oval billiard,  $I(s)$  exhibits a rapid rise at small  $s$ . It is in close agreement with the empirical Poisson curve and supports the systems integrability. While for bean and peanut,  $I(s)$  follows a sigmoidal shape, with clear suppression at  $s \sim 0$ . It closely coincides with the GOE curve, reflecting quantum chaos.

### 1. Level spacing ratio

To strengthen the validity of our results, we employed another commonly used short-range statistical measure, the *level spacing ratio* (LSR)[106, 128–130]. Oganesyan and Huse[131] in 2007 introduced the distribution of the ratios

<sup>17</sup> Data binning or bucketing is a data preprocessing method used to minimize the effects of small observation errors

$r_i$  defined by

$$\langle \tilde{r} \rangle_i = \frac{\min(s_i, s_{i-1})}{\max(s_i, s_{i-1})} = \min(r_i, \frac{1}{r_i}), \quad (17)$$

where

$$r_i = \frac{s_i}{s_{i-1}} \quad (18)$$

is the the ratio of two consecutive level spacings. The notation “ $\min(\dots)$ ” indicates we compute the ratio of the smaller interval to the larger one, ensuring that the resulting value ( $r_i$ ) falls within the range of 0 to 1. The LSR stands out as a convenient and reliable measure of spectral statistics because it avoids the need to unfold the spectrum and is unaffected by local density of states variations. This measure offers a statistical snapshot of the underlying dynamics responsible for the system’s behaviour.

In particular, the mean  $\tilde{r}$  fluctuates around the following values, depending on the distribution of adjacent level spacing in the spectrum being studied [128].

$$\langle \tilde{r} \rangle = \begin{cases} 2 \ln(2) - 1 \approx 0.38629 & \text{Poissonian,} \\ 4 - 2\sqrt{3} \approx 0.5307 & \text{GOE,} \\ \frac{2\sqrt{3}}{\pi} - \frac{1}{2} \approx 0.5996 & \text{GUE} \end{cases} \quad (19)$$

Meanwhile, the average value of  $r$  for Poisson is  $\langle r \rangle_P = \infty$ , whereas for GOE, it is  $\langle r \rangle_{GOE} = 1.75$  [129]. The mean  $\tilde{r}$  and  $r$  for our four billiards are shown in Table (II). Although unfolding is not strictly required, comparing statistics in terms of unfolded energies proves most convenient.

For the Bean and Peanut-shaped billiards, the mean LSR values tend to fluctuate around  $\langle r \rangle_{GOE}$ , indicating chaotic behaviour. In contrast, for the circular and oval billiards, the LSR values hover around  $\langle r \rangle_{Pois}$ , consistent with their integrable nature.

TABLE II. The mean  $\tilde{r}$  and  $r$  for bean-shaped and Cassini ovals billiards.

Billiards	$\langle \tilde{r} \rangle$	Relative error (%)	$\langle r \rangle$	Relative error (%)
Circular	$\sim 0.395968$	2.50	$\rightsquigarrow \infty$ ( $\sim 39895.1$ )	—
Bean	$\sim 0.518245$	3.29	$\sim 1.93933$	10.82
Oval	$\sim 0.382986$	0.86	$\rightsquigarrow \infty$ ( $\sim 16758.6$ )	—
Peanut	$\sim 0.520381$	2.89	$\sim 1.9771$	12.98

### C. Spectral Complexity

Complexity is a real characteristic of a quantum state[132, 133]. Despite its importance, the information embedded within it often disregarded because its intricacies seldom translate into the local observable properties of the system[134]. Complexity in quantum systems is extensive, meaning it scales with the number of active degrees of freedom. Although the examination of spectral complexity[135, 136] originated within the framework of two-dimensional holographic models, this concept has extended beyond holography and has been widely used in diagnosing chaos[137–139]. Specifically, it can be applied to analyse quantum systems with a finite number of degrees of freedom.

In this section, we use spectral complexity to probe chaotic behaviour within billiard systems. Here, the focus is on the time-scale at which the saturation occurs in the growth rate of spectral complexity. In more formal terms, for quantum systems possessing a discrete, non-degenerate energy spectrum, the spectral complexity, denoted as  $C_s(t)$ , is defined as[137, 139]:

$$C_s(t) := \frac{1}{D Z(2\beta)} \sum_{\mathcal{M} \neq \mathcal{N}} \left( \frac{\sin\left(\frac{t(\mathcal{E}_{\mathcal{M}} - \mathcal{E}_{\mathcal{N}})}{2}\right)}{\frac{(\mathcal{E}_{\mathcal{M}} - \mathcal{E}_{\mathcal{N}})}{2}} \right)^2 e^{-\beta(\mathcal{E}_{\mathcal{M}} + \mathcal{E}_{\mathcal{N}})} \quad (20)$$

where  $D$  is the dimension of the Hilbert space  $\mathbb{H}$ ,  $Z(\beta)$  is the thermal partition function,  $\beta = \frac{1}{T}$  is the inverse temperature, and  $\{\mathcal{E}_N\}$  are the discrete energy eigenvalues. Authors[137, 139, 140] have shown that spectral complexity plateaus to different values across different time scales based on the integrability of the system. Specifically, for integrable billiards, the saturation value of  $C_s(t)$  is significantly higher, by orders of magnitude, compared to non-integrable billiard systems. This contrast highlights how spectral complexity stabilisation depends on whether the underlying dynamics are integrable or chaotic. At late times, spectral complexity shows the following behaviours[138],

$$C_s(t) \propto \begin{cases} t & \text{Poissonian,} \\ \ln(t) & \text{GOE,} \\ t^2 & \text{Degenerate Spectra} \end{cases} \quad (21)$$

For quantum systems with non-degenerate energy spectra, the spectral complexity  $C_s(t)$  is constrained due to the property that  $\sin^2\left(\frac{t(\mathcal{E}_M - \mathcal{E}_N)}{2}\right) \leq 1$  in Eq. (20)[138]. This leads to an upper bound on  $C_s(t)$  given by  $\left(\frac{2}{\Delta\mathcal{E}_{min}}\right)^2$ , where  $\Delta\mathcal{E}_{min}$  is the minimum energy level spacing. And at infinite temperature (where  $\beta = 0$ ), the saturation value depends solely on the energy difference  $\Delta\mathcal{E} := \mathcal{E}_M - \mathcal{E}_N$ , not on  $\mathcal{E}_M + \mathcal{E}_N$ . Thus, the saturation value of complexity can reach greater heights when the difference in energy is at its smallest. Therefore,  $\Delta\mathcal{E}_{min}$  represents a key inverse time scale that determines the saturation of spectral complexity.

To make the Hilbert space of an infinite-dimensional quantum system manageable for practical calculations, we truncate it to a finite dimension, specifically setting  $D = 1000$ . This choice of  $D$  is specifically suitable considering, computational time, convergence of  $C_s(t)$ , and resolution between different temperatures. For a quantum system with  $D$ -dimensional Hilbert space and non-degenerate energy spectrum, the number of distinct lowest energy eigenvalues  $N$  can match the truncated Hilbert space dimension  $D$ [141]. For computing spectral complexity, the essential component is the energy spectrum, which we obtain numerically following Eq. (15).

Here, in Fig. (13), we observe a clear distinction in the late-time behaviour of  $C_s(t)$  between different billiard shapes. Specifically, for integrable billiards with circular (Fig. (13(a))) and oval (Fig. (13(c))) shapes, the spectral complexity saturates at a noticeably later timescale than for non-integrable billiards with bean (Fig. (13(b))) and peanut (Fig. (13(d))) shapes. In chaotic (non-integrable) systems, level repulsion, the tendency for energy levels to avoid crossing or clustering, prevents the energy difference  $\Delta\mathcal{E}_{min}$  from approaching zero. As a result, the saturation timescales for spectral complexity in chaotic systems are significantly shorter than those observed in integrable systems, revealing a disparity of several orders of magnitude.

In addition, as the temperature is lowered, the  $C_s(t)$  decreases for both the bean and peanut billiard shapes. This behaviour shows how temperature affects the growth of complexity, indicating that chaotic systems become less complex at lower temperatures. However, for integrable billiards with circular and oval shapes, the behaviour of  $C_s(t)$  remains relatively stable across varying temperatures. This consistency suggests that in integrable systems, complexity is less sensitive to thermal effects, pointing to a fundamental difference in how integrable and chaotic systems respond to temperature fluctuations in terms of complexity growth.

## V. DISCUSSION AND CONCLUSION

This study investigates the dynamics of billiard systems defined by boundaries that feature both positive and negative curvatures—specifically, a bean-shaped billiard and a peanut-shaped billiard. Unlike conventional chaotic billiards, these systems include both focusing and defocusing boundary segments with no neutral regions. This unique boundary structure leads to a mix of chaotic and regular trajectories, making these systems valuable for exploring the relationship between classical and quantum chaos. Our analysis focused on key aspects of chaotic behaviour and its quantum signatures, including the billiard flow, billiard maps, eigenfunction scarring, level spacing distribution, and spectral complexity. By integrating these classical and quantum descriptions, we are able to offer a comprehensive perspective on how chaotic dynamics manifest across both frameworks, highlighting the nuanced relationship between classical chaos and its quantum counterparts.

The circular or oval billiards fall outside EH, for they are inherently non-ergodic. Conversely, billiards with dispersing boundaries and hyperbolic dynamics (such as bean-shaped or peanut-shaped billiards) exhibit enough structural complexity to potentially reach higher levels in the hierarchy. We intend to investigate the nature of ergodicity in a separate study.

In circular and oval billiards, invariant curves cover the phase space completely. These curves represent the trajectories that particles strictly follow without deviating or mixing with others, thereby preserving a highly ordered motion. This results in predictable, periodic behaviour, characteristic of integrable systems, where dynamics remain

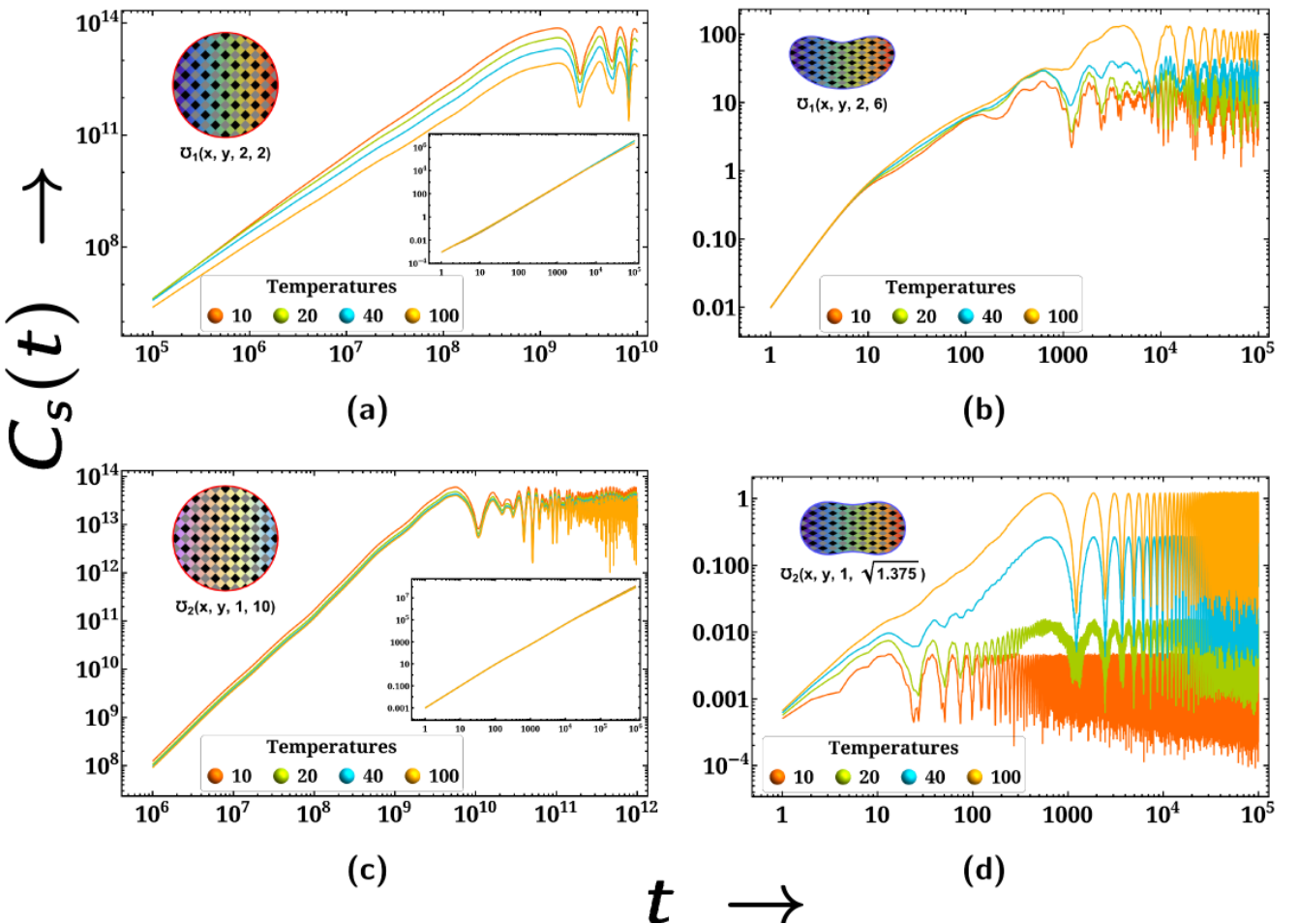


FIG. 13. Temperature dependence of spectral complexity at  $T = 10, 20, 40, 100$  for (a) Circle, (b) Bean (c) Oval and (d) Peanut billiards. As expected, Bean and Peanut Billiards exhibit logarithmic late-time growth consistent with the GOE. Conversely, Circular and Oval billiards show linear late-time growth, mirroring the expected behaviour of a Poisson spectrum.

entirely regular and free from chaos. In contrast, the flow diagrams for the bean-shaped and peanut-shaped billiards are filled with irregular and unpredictable trajectories.

The classical chaotic behaviour in billiards is vivid when examining the billiard maps. In general, billiard systems exhibit mixed behaviours, akin to other Hamiltonian systems, with regions of invariant tori interwoven with the chaotic sea. In these maps, densely scattered, non-repeating points are a strong indicator of chaos, while smooth, repetitive patterns point towards regular and predictable motion. For instance, for bean-shaped and peanut-shaped billiards, the billiard maps display a complex blend of regular and chaotic regions. In contrast, circular and oval billiards show evenly spaced points that form patterns like horizontal lines, horizontal waves, or closed loops. These indicate the absence of chaos, aligning with their integrable nature.

This observation is essential as it helps visualising the transition zones where classical chaos can impact quantum behaviour. In chaotic regions of the phase space, we expect quantum manifestations like level repulsion and complex wave function patterns, aligning with RMT predictions. In contrast, regular regions with invariant tori suggest quantised energy levels that tend to cluster or display Poisson-like distributions, reflecting the ordered nature of the underlying classical dynamics. Understanding these zones provides insight into the interplay between classical and quantum chaos.

In quantum mechanics, the associated Hilbert space is infinite-dimensional, accommodating the various states of the system. To analyse chaotic properties more effectively, we often truncate the spectrum to a finite number of states, limiting our attention to a finite set of degrees of freedom. This truncation enables us to the study of chaotic dynamics within a manageable framework while retaining the essential properties of the quantum system.

Our observations revealed eigenfunction scarring, a remarkable quantum phenomenon. A classical chaotic system, despite its generally unpredictable nature, can exhibit hidden periodic behaviour for certain ICs, where the system fol-

lows a closed, repeating trajectory. In the corresponding quantum system, these closed trajectories produce noticeable high-density imprints on certain steady-state eigenfunctions, known as scars[142]. Eigenfunction scarring provides a direct quantum signature of classical chaotic trajectories. The persistence of scarred eigenfunctions, particularly in regions of phase space associated with slow diverging trajectories, indicates that even in the quantum domain, remnants of classical dynamics significantly shape the system's behaviour. In both the billiard models, we find scarred and super scarred states. When both types of localisation coexist, understanding the interplay between chaos and symmetry of the system becomes important. The scarring reflects the underlying chaotic dynamics, while super scars reveal how symmetries or special constraints constrain the system's behaviour. This coexistence can influence the system's physical properties, such as energy level statistics, transport properties, or resonance behaviour, particularly in systems where both chaos and order are intertwined. Scarring phenomena highlight the rich and intricate behaviour of quantum systems, and serves as a visual manifestation of quantum and classical correspondence, as well as a demonstration of the quantum suppression chaos at a local level.

The examination of the level spacing distribution in the quantum billiard aligns closely with the theoretical framework of RMT. For classically regular (circular and oval) and chaotic (bean and peanut) billiards, the NNSD exhibits Poisson and GOE (WD) distributions, respectively. While the former distribution is the hallmark of integrable systems, the latter stands for chaos. Just like NNSD, the cumulative level-spacing distribution also provides critical insights into the spectral properties of these quantum systems. As expected, we find,  $I(S)$  follows Poissonian statics for Circular and Oval-shaped billiard, indicating no level repulsion and uncorrelated energy levels. But for Bean and Peanut,  $I(S)$  follows WD statics, indicative of strong level repulsion, and hence quantum chaos. Furthermore, the mean LSR values shown in Table (II) confirm the previous conclusions about the level spacing distributions. These results suggest that the chaotic dynamics observed in classical systems can affect the statistical behaviour of quantum energy levels. This connection matters in bringing together classical and quantum mechanics, particularly in the study of chaotic systems.

TABLE III. Area and boundary length of the Billiards

Billiards	$ \Omega $	$ d\Omega $
Circular:	$4\pi$	$4\pi$
Bean:	31.4159	22.2411
Oval:	314.151	62.8322
Peanut:	3.67382	7.68519

Another statistical measure is the spectral staircase function (or the level counting function),  $N(\mathcal{E})$ , provides a count of the eigenstates (or modes) with energies less than or equal to a specified energy value  $\mathcal{E}$  [106, 143, 144]. Mathematically,  $N(\mathcal{E}) := \#\{\mathcal{N} \in \mathbb{N} \mid \mathcal{E}_{\mathcal{N}} \leq \mathcal{E}\}$ . The spectral staircase for billiards has an asymptotic mean. This mean is given by the well-known generalised Weyl's law[145–147],  $N_{Weyl}(\mathcal{E}) = \left( \frac{|\Omega| (2 \mathcal{E})^{\frac{d}{2}} + |d\Omega| (2 \mathcal{E})^{\frac{d-1}{2}}}{4\pi} \right) + \mathcal{R}(\mathcal{E})$ ,

where  $d$  is the system's spatial dimension,  $|\Omega|$  denotes the area of the billiard,  $|d\Omega|$  is the length of the boundary provided in Table (III) and  $\mathcal{R}(\mathcal{E})$  is the remainder term, representing higher-order corrections. In cases where the boundary is sufficiently regular (e.g., smooth), the first two terms dominate, and the remainder  $\mathcal{R}(\mathcal{E})$  decays rapidly. For domains with singularities (e.g., corners, edges or cusps),  $\mathcal{R}(\mathcal{E})$  is more complicated and depends on the geometric details of the singularities and may grow more slowly than the smooth-boundary case but cannot exceed  $\mathcal{O}(\mathcal{E}^{\frac{d-1}{2}})$ . Here, instead of  $\mathcal{E}$  in the numerator, we have used  $2\mathcal{E}$  in accordance with Eq (15) where we have considered  $m = 1$ , not  $2m = 1$ . Therefore, the spectral staircase function is amenable to separation into two parts.

1. The smooth part,  $(N_{Weyl}(\mathcal{E}))$ : This represents the mean density of states and is dictated by the geometric characteristics of the system (e.g. area, perimeter, or volume).
2. The fluctuating part  $(N(\mathcal{E}))$ : It captures oscillatory deviations from the smooth part strongly influenced by classical periodic orbits (via the Gutzwiller trace formula) and quantum chaos.

In integrable systems,  $N(\mathcal{E})$  grows smoothly with small, regular fluctuations. This shows that the level spacing is uniform. On the other hand, chaotic systems have irregular and complex fluctuations in  $N(\mathcal{E})$ , indicating non-uniform level spacing. These irregular fluctuations are often connected to phenomena like quantum interference and the scarring of wavefunctions along classical unstable periodic orbits. In Fig. (14), we present the spectral staircase

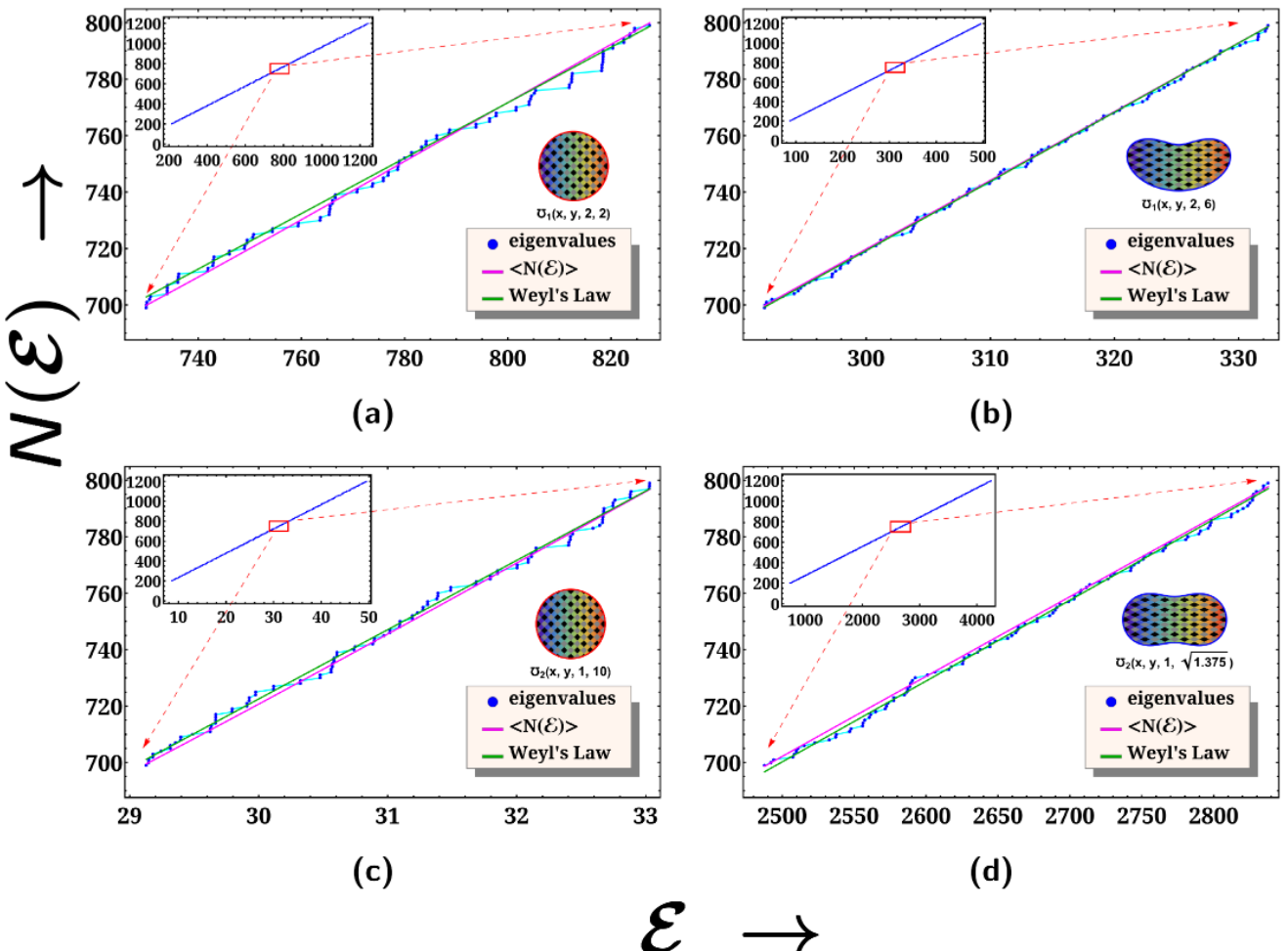


FIG. 14. The plot displays the spectral staircase function  $N(\epsilon)$ , with its characteristic steps corresponding to discrete eigenvalues. While the red line provides the overall trend, the green line corresponds to Weyl's law. Both the lines are seen to describe the average behaviour of  $N(\epsilon)$ , reasonably well.  $N \in [700, 800]$

function, which adequately highlights the contrasting characteristics of integrable and chaotic behaviour in our billiard models. The spectral staircase functions for circular (Fig. (14(a))) and oval (Fig. (14(c))) billiards exhibit nearly identical growth patterns, with small fluctuating steps arranged in a relatively regular manner. In contrast, for bean-shaped (Fig. (14(b))) and peanut-shaped (Fig. (14(d))) billiards, the staircase function fluctuates irregularly with uneven intervals, providing a distinct signature of chaos.

Besides conventional methods for diagnosing chaos, our analysis of the time evolution of spectral complexity across four billiard models revealed striking differences between them. It captures both short-time and long-time behaviour. Spectral complexity unifies time dynamics, thermal effects, and spectral rigidity into a single framework, offering a sharper probe of quantum chaos than static metrics. Its temperature dependence is particularly powerful. The inverse temperature  $\beta$  in  $C_s(t)$  acts as a thermal filter:

1. High temperatures ( $\beta \rightarrow 0$ ): All energy levels contribute equally, probing global spectral correlations.
2. Low temperatures ( $\beta \gg 1$ ): Suppresses high-energy states, isolating low-energy dynamics.

In all cases, spectral complexity initially increases according to the relationship  $C_s(t) \propto c_1 \log\left(\cosh\left(\frac{c_2 t}{\beta}\right)\right)$  capturing a period of rapid growth. However, following this initial phase, growth ceases and the spectral complexity fluctuates erratically around a constant value, a phenomenon we label ‘saturation’. Interestingly, we observe that saturation occurs much sooner in chaotic systems, like the bean- and peanut-shaped billiards, compared to the integrable systems, such as the circular and oval billiards. This early saturation in chaotic systems suggests a faster

transition to complexity, reflecting the underlying chaotic nature compared to the gradual, regular build-up seen in integrable systems. This dichotomy makes it a powerful tool to distinguish chaos from regularity.

The temperature dependency in spectral complexity also provides insight into how thermal effects interact with quantum chaos. Here, we find that the spectral complexity decreases as the temperature decreases across both chaotic and integrable billiards. However, in circular and oval billiards (integrable systems), spectral complexity shows minimal sensitivity to temperature changes, with the saturation point remaining nearly identical for small values of  $\mathcal{N}$ . Here, the parameter  $\mathcal{N}$  serves as a resolution parameter. This is because spectral complexity, in its definition, has input from the full spectrum of the system. In contrast, in the chaotic billiards, the temperature has a more pronounced impact. At higher temperatures, spectral complexity grows substantially and saturates at a much higher value and over a longer timescale compared to lower temperatures. At low temperatures, spectral complexity saturates at an earlier time, reaching a low value. This temperature-dependent behaviour aligns with the idea that lower temperatures lead to exponential suppression of complexity, as described by Eq. (21), which constrains the growth of spectral complexity. This examination highlights the impact of thermal fluctuations on chaotic systems and highlighting how temperature modulates quantum chaotic behaviour across different types of billiards.

Our results are consistent with earlier studies on chaotic billiards, such as those investigating quantum chaos in stadium billiards. However, our work expands on these findings by providing new insights into the role of eigenfunction scarring in systems with mixed phase space and by using a novel approach to map classical Poincaré dynamics onto quantum phenomena. These findings suggest that, while there is strong evidence of classical-quantum correspondence, specific system geometries and boundary conditions can lead to nuanced behaviour not previously explored in depth.

In the present work we have modelled two new chaotic domains with mixed curvatures and demonstrate the universal responses of quantum systems with classically chaotic dynamics.

Our analysis demonstrates a clear correspondence between classical chaotic behaviour and quantum manifestations in billiard systems. Chaotic billiards display significant quantum complexity, marked by eigenfunction scarring, level repulsion, and high spectral complexity, aligning well with classical chaos indicators. The contrast between regular and chaotic billiards highlights how quantum mechanics can mirror classical dynamics, with distinct quantum signatures emerging from chaotic trajectories. This study underscores the nuanced interplay between order and chaos, both classically and quantum mechanically, showing that thermal effects and spectral complexity offer additional insight into quantum chaos. By bridging classical and quantum perspectives, we contribute to a deeper understanding of chaotic dynamics across different domains, offering a foundation for future studies on the transition between regularity and chaos in complex systems.

The properties of mechanical reflection closely mirror those of optical reflection. Consequently, the path of a light ray bouncing inside a cavity with perfectly reflective inner walls resembles the trajectory of a point particle moving within the same cavity. This similarity makes chaotic models valuable for designing light-trapping devices, which are beneficial in applications like solar energy harvesting [148, 149]. Understanding the internal trajectories of light rays in various geometrical cavities could play a significant role in maximising energy transfer from solar radiation to an absorbing material, which could potentially coat the inner walls of such cavities. Furthermore, the exploration of chaotic billiard systems with mixed curvatures can have practical applications in designing and optimising microfluidic devices, optical cavities, and other structures that rely on the manipulation of particles or waves within confined spaces.

## ACKNOWLEDGMENTS

The authors extend their gratitude to Subhash Chandra Mahapatra for his generous provision of computational resources, which greatly aided in a portion of the numerical computations.

- [1] A. Bäcker, “Eigenfunctions in chaotic quantum systems,” 2007. [1](#)
- [2] M. Berry, “Quantum chaology, not quantum chaos,” *Physica Scripta*, vol. 40, p. 335, sep 1989.
- [3] M. V. Berry, I. C. Percival, and N. O. Weiss, “The bakerian lecture, 1987. quantum chaology,” *Proceedings of the Royal Society of London. A. Mathematical and Physical Sciences*, vol. 413, no. 1844, pp. 183–198, 1987. [1](#)
- [4] E. D. Leonel, *Introduction to Billiard Dynamics*, pp. 171–180. Singapore: Springer Singapore, 2021. [1, 10](#)
- [5] Y. G. Sinai, “What is ... a billiard,” *Notices Amer. Math. Soc.*, vol. 51, pp. 412–413, 2004.
- [6] H. Poritsky, “The billiard ball problem on a table with a convex boundary—an illustrative dynamical problem,” *Annals of Mathematics*, vol. 51, no. 2, pp. 446–470, 1950.
- [7] M. Bialy and A. E. Mironov, “The Birkhoff-Poritsky conjecture for centrally-symmetric billiard tables,” *Annals of Mathematics*, vol. 196, no. 1, pp. 389 – 413.

- [8] N. Chernov and R. Markarian, *Chaotic Billiards*. Mathematical surveys and monographs, American Mathematical Society, 2006. 1, 3, 7, 11
- [9] H. J. Korsch and F. Zimmer, *Chaotic Billiards*, pp. 15–36. Berlin, Heidelberg: Springer Berlin Heidelberg, 2002. 1, 15
- [10] T. Albers, S. Delnoij, N. Schramma, and M. Jalaal, “Billiards with spatial memory,” *Phys. Rev. Lett.*, vol. 132, p. 157101, Apr 2024. 1
- [11] A. Bernardo, “181. Nonlinear Dynamics and Chaos: an Introduction - Matematicamente,” 4 2013. 2
- [12] G. Casati and T. Prosen, “The quantum mechanics of chaotic billiards,” *Physica D: Nonlinear Phenomena*, vol. 131, no. 1, pp. 293–310, 1999. Classical Chaos and its Quantum Manifestations. 2
- [13] E. Ott, *Chaos in Dynamical Systems*. Cambridge University Press, 2002. 2
- [14] N. Chernov and R. Markarian, *Chaotic Billiards*. Mathematical Surveys and Monographs, American Mathematical Society, 2023. 2, 9
- [15] R. Frigg, J. Berkovitz, and F. Kronz, “The Ergodic Hierarchy,” in *The Stanford Encyclopedia of Philosophy* (E. N. Zalta, ed.), Metaphysics Research Lab, Stanford University, Fall 2020 ed., 2020.
- [16] J. Berkovitz, R. Frigg, and F. Kronz, “The ergodic hierarchy, randomness and hamiltonian chaos,” *Studies in History and Philosophy of Science Part B: Studies in History and Philosophy of Modern Physics*, vol. 37, no. 4, pp. 661–691, 2006. 2
- [17] L. A. Bunimovich, Y. G. Sinai, and N. I. Chernov, “Statistical properties of two-dimensional hyperbolic billiards,” *Russian Mathematical Surveys*, vol. 46, no. 4, p. 47, 1991. 3
- [18] Y. G. Sinai, “On the foundations of the ergodic hypothesis for a dynamical system of statistical mechanics,” in *Doklady Akademii Nauk*, vol. 153, pp. 1261–1264, Russian Academy of Sciences, 1963.
- [19] Y. G. Sinai, “Dynamical systems with elastic reflections,” *Russian Mathematical Surveys*, vol. 25, no. 2, p. 137, 1970. 3
- [20] B. Moran, W. G. Hoover, and S. Bestiale, “Diffusion in a periodic lorentz gas,” *Journal of Statistical Physics*, vol. 48, pp. 709–726, 1987. 3
- [21] L. A. Bunimovich, “On ergodic properties of certain billiards,” *Functional Analysis and Its Applications*, vol. 8, no. 3, pp. 254–255, 1974. 3
- [22] L. A. Bunimovich, “Conditions of stochasticity of two-dimensional billiards,” *Chaos: An Interdisciplinary Journal of Nonlinear Science*, vol. 1, no. 2, pp. 187–193, 1991. 3
- [23] E. G. Altmann, J. S. E. Portela, and T. Tél, “Leaking chaotic systems,” *Rev. Mod. Phys.*, vol. 85, pp. 869–918, May 2013. 3
- [24] G. Harris, “Polygonal billiards,” *Southern Illinois university Edwardsville*, vol. 87, p. 88, 2007. 3
- [25] E. B. Rozenbaum, L. A. Bunimovich, and V. Galitski, “Early-time exponential instabilities in nonchaotic quantum systems,” *Phys. Rev. Lett.*, vol. 125, p. 014101, Jul 2020.
- [26] J. Wang, G. Benenti, G. Casati, and W.-g. Wang, “Quantum chaos and the correspondence principle,” *Phys. Rev. E*, vol. 103, p. L030201, Mar 2021.
- [27] F. Leyvraz, C. Schmit, and T. H. Seligman, “Anomalous spectral statistics in a symmetrical billiard,” *Journal of Physics A: Mathematical and General*, vol. 29, p. L575, nov 1996. 3
- [28] M. Wojtkowski, “Principles for the design of billiards with nonvanishing lyapunov exponents,” *Communications in Mathematical Physics*, vol. 105, pp. 391–414, Sep 1986. 3, 4
- [29] M. Berry, “Improved eigenvalue sums for inferring quantum billiard geometry,” *Journal of Physics A: Mathematical and General*, vol. 20, no. 9, p. 2389, 1987. 3
- [30] M. V. Berry and R. J. Mondragon, “Neutrino billiards: time-reversal symmetry-breaking without magnetic fields,” *Proceedings of the Royal Society of London. A. Mathematical and Physical Sciences*, vol. 412, no. 1842, pp. 53–74, 1987.
- [31] B. Dietz, T. Klaus, M. Miski-Oglu, A. Richter, M. Wunderle, and C. Bouazza, “Spectral properties of dirac billiards at the van hove singularities,” *Phys. Rev. Lett.*, vol. 116, p. 023901, Jan 2016.
- [32] C. Dembowski, B. Dietz, H.-D. Gräf, A. Heine, F. Leyvraz, M. Miski-Oglu, A. Richter, and T. H. Seligman, “Phase shift experiments identifying kramers doublets in a chaotic superconducting microwave billiard of threefold symmetry,” *Phys. Rev. Lett.*, vol. 90, p. 014102, Jan 2003.
- [33] W. Zhang and B. Dietz, “Microwave photonic crystals, graphene, and honeycomb-kagome billiards with threefold symmetry: Comparison with nonrelativistic and relativistic quantum billiards,” *Phys. Rev. B*, vol. 104, p. 064310, Aug 2021.
- [34] W. Zhang, X. Zhang, J. Che, M. Miski-Oglu, and B. Dietz, “Properties of eigenmodes and quantum-chaotic scattering in a superconducting microwave dirac billiard with threefold rotational symmetry,” *Phys. Rev. B*, vol. 107, p. 144308, Apr 2023.
- [35] W. Zhang and B. Dietz, “Graphene billiards with fourfold symmetry,” *Phys. Rev. Res.*, vol. 5, p. 043028, Oct 2023. 3
- [36] H. M. Cundy and A. P. Rollett, *Mathematical models*. Clarendon Press, Oxford, 1961. 2nd ed. 3, 4
- [37] V. S. Vaze, S. Schönfelder, and K. W. Axhausen, “Continuous space representations of human activity spaces,” *Arbeitsberichte Verkehrs-und Raumplanung*, vol. 295, 2005. 4, 5
- [38] E. W. Weisstein, “Bean curve.”
- [39] E. Weisstein, *CRC Concise Encyclopedia of Mathematics*. CRC Press, 2002. 3, 4, 5
- [40] G. Carlo, E. Vergini, and A. J. Fendrik, “Numerical verification of percival’s conjecture in a quantum billiard,” *Phys. Rev. E*, vol. 57, pp. 5397–5403, May 1998. 3
- [41] M. Karataş, “A multi foci closed curve: Cassini oval, its properties and applications,” *Doğuş Üniversitesi Dergisi*, vol. 14, no. 2, pp. 231–248, 2013.
- [42] R. Kress, F. Yaman, A. Yapar, and I. Akduman, “Inverse scattering for an impedance cylinder buried in a dielectric cylinder,” *Inverse Problems in Science and Engineering*, vol. 17, no. 4, pp. 473–488, 2009. 3

- [43] W. T. Lu, W. Zeng, and S. Sridhar, “Duality between quantum and classical dynamics for integrable billiards,” *Phys. Rev. E*, vol. 73, p. 046201, 2006. [4](#)
- [44] M. Sieber and F. Steiner, “Classical and quantum mechanics of a strongly chaotic billiard system,” *Physica D*, vol. 44, pp. 248–266, 1990. [4](#)
- [45] C. Gibson, *Elementary Geometry of Algebraic Curves: An Undergraduate Introduction*. Elementary Geometry of Algebraic Curves: An Undergraduate Introduction, Cambridge University Press, 1998. [4](#)
- [46] E. W. Weisstein. [5](#)
- [47] E. Abbena, S. Salamon, and A. Gray, *Modern Differential Geometry of Curves and Surfaces with Mathematica*. Textbooks in Mathematics, CRC Press, 2017. [6](#)
- [48] J. Lawrence, *A Catalog of Special Plane Curves*. Dover Books on Mathematics, Dover Publications, 1972.
- [49] R. Yates, *A Handbook on Curves and Their Properties*. J.W. Edwards, 1947.
- [50] E. Lockwood, *A Book of Curves*. University Press, 1967.
- [51] T. Needham, *Visual complex analysis*. Oxford University Press, 2023. [6](#)
- [52] P. Popescu-Pampu, *Jakob Bernoulli and the Construction of Curves*, pp. 11–13. Cham: Springer International Publishing, 2016. [6](#)
- [53] P. Grabusts and O. Uzhga-Rebrov, “Applications of the symmetrical structures of cassini ovals,” *Symmetry*, vol. 16, no. 3, 2024. [6](#)
- [54] M. Skolnik, *Introduction to Radar Systems*. McGraw-Hill Education, 2002.
- [55] N. Willis, *Bistatic Radar*. Artech House radar library, Institution of Engineering and Technology, 2005. [6](#)
- [56] E. Brieskorn, H. Knörrer, and J. Stillwell, *Plane Algebraic Curves: Translated by John Stillwell*. Modern Birkhäuser Classics, Springer Basel, 2012. [6](#)
- [57] D. Wells, *The Penguin Dictionary of Curious and Interesting Geometry*. Penguin book, Penguin Books, 1991. [6](#)
- [58] L. Moroni, “The toric sections: a simple introduction,” 2017. [6](#)
- [59] S. Strogatz and M. Dichter, *Nonlinear Dynamics and Chaos, 2nd ed. SET with Student Solutions Manual*. Studies in Nonlinearity, Avalon Publishing, 2016. [6](#)
- [60] E. Lorenz, “Predictability: Does the flap of a butterfly’s wing in brazil set off a tornado in texas?,” 1972.
- [61] B. Sivakumar, *Fundamentals of Chaos Theory*, pp. 149–171. Dordrecht: Springer Netherlands, 2017. [6](#)
- [62] M. Himmelstrand and V. Wilén, “A survey of dynamical billiards,” 2013. [7](#)
- [63] K. Gustafson, “Domain decomposition, operator trigonometry, robin condition,” *Contemporary Mathematics*, vol. 218, pp. 432–437, 1998. [7](#)
- [64] A. Bäcker, “Quantum chaos in billiards,” *Computing in Science & Engineering*, vol. 9, 2007. [7, 16](#)
- [65] V. Kaloshin and A. Sorrentino, “On the integrability of birkhoff billiards,” *Philosophical Transactions of the Royal Society A: Mathematical, Physical and Engineering Sciences*, vol. 376, no. 2131, p. 20170419, 2018. [9](#)
- [66] J. Bruce, P. Giblin, and C. Gibson, “Caustics through the looking glass,” *The Mathematical Intelligencer*, vol. 6, pp. 47–58, 1984. [9](#)
- [67] N. Hungerbühler, “The inverse caustic problem,” *The American Mathematical Monthly*, vol. 127, no. 5, pp. 387–400, 2020. [9](#)
- [68] M. Berry and C. Upstill, “Iv catastrophe optics: Morphologies of caustics and their diffraction patterns,” vol. 18 of *Progress in Optics*, pp. 257–346, Elsevier, 1980. [9](#)
- [69] M. Gutzwiller, *Chaos in Classical and Quantum Mechanics*. Springer, 2014. [9](#)
- [70] M. V. Berry, “Evolution of semiclassical quantum states in phase space,” *Journal of Physics A: Mathematical and General*, vol. 12, p. 625, may 1979. [10](#)
- [71] P. Cvitanovic, R. Artuso, R. Mainieri, G. Tanner, G. Vattay, N. Whelan, and A. Wirzba, *Chaos: classical and quantum*, vol. 69, 2005. [10](#)
- [72] J. Leys, É. Ghys, and A. Alvarez, “Chapter V : Billiards - Duhem’s bull,” in *Chaos – A Mathematical Adventure*, Lyon: École normale supérieure de Lyon, 2013.
- [73] L. Seemann, J. Lukin, M. Häßler, S. Gemming, and M. Hentschel, “Complex dynamics in circular and deformed bilayer graphene-inspired billiards with anisotropy and strain,” *Symmetry*, vol. 17, no. 2, 2025.
- [74] T. P. Leonid A. Bunimovich, Giulio Casati and G. Vidmar, “Few islands approximation of hamiltonian system with divided phase space,” *Experimental Mathematics*, vol. 30, no. 4, pp. 459–468, 2021. [10](#)
- [75] G. Datseris and U. Parlitz, *Billiards, Conservative Systems and Ergodicity*, pp. 121–136. Cham: Springer International Publishing, 2022. [11](#)
- [76] T. Iitaka, J. Bird, M. Stopa, K. Ishibashi, Y. Aoyagi, and T. Sugano, “Phase breaking in a quantum billiard,” *International Journal of Bifurcation and Chaos*, vol. 07, no. 04, pp. 937–943, 1997. [11](#)
- [77] M. Mikhailov, “Finite difference method by using mathematica,” *International Journal of Heat and Mass Transfer*, vol. 37, pp. 375–379, 1994. [13](#)
- [78] S. K. Godunov and I. Bohachevsky, “Finite difference method for numerical computation of discontinuous solutions of the equations of fluid dynamics,” *Matematicheskij sbornik*, vol. 47, no. 3, pp. 271–306, 1959.
- [79] T. Liszka and J. Orkisz, “The finite difference method at arbitrary irregular grids and its application in applied mechanics,” *Computers & Structures*, vol. 11, no. 1-2, pp. 83–95, 1980. [13](#)
- [80] M. D. Mikhailov, “Finite element method by using mathematica,” in *Mathematical Modelling Courses for Engineering Education* (Y. Ersoy and A. O. Moscardini, eds.), (Berlin, Heidelberg), pp. 129–151, Springer Berlin Heidelberg, 1994. [13](#)
- [81] S. S. Rao, *The finite element method in engineering*. Elsevier, 2010.

- [82] G. Nikishkov, “Introduction to the finite element method,” *University of Aizu*, pp. 1–70, 2004.
- [83] J. N. Reddy, “An introduction to the finite element method,” *New York*, vol. 27, p. 14, 1993. [13](#)
- [84] M. Sieber and F. Steiner, “Quantum chaos in the hyperbola billiard,” *Phys. Lett. A*, vol. 148, pp. 415–420, 1990. [13](#)
- [85] A. H.-D. Cheng and D. T. Cheng, “Heritage and early history of the boundary element method,” *Engineering analysis with boundary elements*, vol. 29, no. 3, pp. 268–302, 2005.
- [86] G. Beer, I. Smith, and C. Duenser, *The boundary element method with programming: for engineers and scientists*. Springer Science & Business Media, 2008.
- [87] Y. Liu, S. Mukherjee, N. Nishimura, M. Schanz, W. Ye, A. Sutradhar, E. Pan, N. A. Dumont, A. Frangi, and A. Saez, “Recent advances and emerging applications of the boundary element method,” *Applied Mechanics Reviews*, vol. 64, no. 3, p. 030802, 2011. [13](#)
- [88] A. I. Shnirel'man, “Ergodic properties of eigenfunctions,” *Uspekhi Matematicheskikh Nauk*, vol. 29, no. 6, pp. 181–182, 1974. [14](#)
- [89] A. Shnirelman, *The True Story of Quantum Ergodic Theorem*, pp. 245–257. Cham: Springer International Publishing, 2023.
- [90] S. Zelditch, “Uniform distribution of eigenfunctions on compact hyperbolic surfaces,” *Duke Mathematical Journal*, vol. 55, no. 4, pp. 919 – 941, 1987.
- [91] S. Zelditch, “Quantum ergodicity and mixing,” *arXiv preprint math-ph/0503026*, 2005.
- [92] T. Sunada, “Quantum ergodicity,” in *Progress in inverse spectral geometry*, pp. 175–196, Springer, 1997. [14](#)
- [93] S. W. McDonald, “Wave dynamics of regular and chaotic rays,” [14](#)
- [94] E. J. Heller, “Bound-state eigenfunctions of classically chaotic hamiltonian systems: Scars of periodic orbits,” *Phys. Rev. Lett.*, vol. 53, pp. 1515–1518, Oct 1984. [14](#)
- [95] C. J. Turner, A. A. Michailidis, D. A. Abanin, M. Serbyn, and Z. Papić, “Weak ergodicity breaking from quantum many-body scars,” *Nature Physics*, vol. 14, no. 7, pp. 745–749, 2018.
- [96] B. Bhattacharjee, S. Sur, and P. Nandy, “Probing quantum scars and weak ergodicity breaking through quantum complexity,” *Phys. Rev. B*, vol. 106, p. 205150, Nov 2022.
- [97] M. V. Berry, “Quantum scars of classical closed orbits in phase space,” *Proceedings of the Royal Society of London. A. Mathematical and Physical Sciences*, vol. 423, no. 1864, pp. 219–231, 1989.
- [98] L. Huang, Y.-C. Lai, D. K. Ferry, S. M. Goodnick, and R. Akis, “Relativistic quantum scars,” *Phys. Rev. Lett.*, vol. 103, p. 054101, Jul 2009.
- [99] B. Evrard, A. Pizzi, S. I. Mistakidis, and C. B. Dag, “Quantum scars and regular eigenstates in a chaotic spinor condensate,” *Phys. Rev. Lett.*, vol. 132, p. 020401, Jan 2024. [14](#)
- [100] M. Srednicki, “Chaos and quantum thermalization,” *Physical review e*, vol. 50, no. 2, p. 888, 1994. [14](#)
- [101] A. Pizzi, “Quantum trails and memory effects in the phase space of chaotic quantum systems,” 2024. [14](#)
- [102] A. M. Graf, J. Keski-Rahkonen, M. Xiao, S. Atwood, Z. Lu, S. Chen, and E. J. Heller, “Birthmarks: Ergodicity breaking beyond quantum scars,” 2024. [14](#)
- [103] E. Bogomolny and C. Schmit, “Structure of wave functions of pseudointegrable billiards,” *Phys. Rev. Lett.*, vol. 92, p. 244102, Jun 2004. [14](#)
- [104] S. Åberg, T. Guhr, M. Miski-Oglu, and A. Richter, “Superscars in billiards: A model for doorway states in quantum spectra,” *Phys. Rev. Lett.*, vol. 100, p. 204101, May 2008.
- [105] E. Bogomolny, “Formation of superscar waves in plane polygonal billiards\*,” *Journal of Physics Communications*, vol. 5, p. 055010, may 2021.
- [106] i. c. v. Lozej, G. Casati, and T. c. v. Prosen, “Quantum chaos in triangular billiards,” *Phys. Rev. Res.*, vol. 4, p. 013138, Feb 2022. [18](#), [22](#)
- [107] E. Bogomolny, B. Dietz, T. Friedrich, M. Miski-Oglu, A. Richter, F. Schäfer, and C. Schmit, “First experimental observation of superscars in a pseudointegrable barrier billiard,” *Phys. Rev. Lett.*, vol. 97, p. 254102, Dec 2006.
- [108] S. R. Jain and R. Samajdar, “Nodal portraits of quantum billiards: Domains, lines, and statistics,” *Rev. Mod. Phys.*, vol. 89, p. 045005, Dec 2017. [14](#)
- [109] E. Bogomolny, “Smoothed wave functions of chaotic quantum systems,” *Physica D: Nonlinear Phenomena*, vol. 31, no. 2, pp. 169–189, 1988. [14](#)
- [110] J. Keski-Rahkonen, P. J. J. Luukko, S. Åberg, and E. Räsänen, “Effects of scarring on quantum chaos in disordered quantum wells,” *Journal of Physics: Condensed Matter*, vol. 31, p. 105301, jan 2019. [15](#)
- [111] T. Guhr, A. Müller-Groeling, and H. A. Weidenmüller, “Random-matrix theories in quantum physics: common concepts,” *Physics Reports*, vol. 299, no. 4, pp. 189–425, 1998. [16](#)
- [112] R. J. Zijderveld, A. M. Bozkurt, M. Wimmer, and İnanç Adagideli, “Quantum scars and caustics in Majorana billiards,” *SciPost Phys.*, vol. 17, p. 147, 2024. [16](#)
- [113] O. Bohigas, M. J. Giannoni, and C. Schmit, “Characterization of chaotic quantum spectra and universality of level fluctuation laws,” *Phys. Rev. Lett.*, vol. 52, pp. 1–4, Jan 1984. [16](#), [17](#)
- [114] F. J. Dyson, “Statistical Theory of the Energy Levels of Complex Systems. I,” *Journal of Mathematical Physics*, vol. 3, pp. 140–156, 01 1962. [16](#)
- [115] F. J. Dyson, “Statistical Theory of the Energy Levels of Complex Systems. II,” *Journal of Mathematical Physics*, vol. 3, pp. 157–165, 01 1962. [17](#)
- [116] F. J. Dyson, “Statistical Theory of the Energy Levels of Complex Systems. III,” *Journal of Mathematical Physics*, vol. 3, pp. 166–175, 01 1962. [16](#)
- [117] M. V. Berry, “Regular and irregular semiclassical wavefunctions,” *Journal of Physics A: Mathematical and General*,

- vol. 10, p. 2083, dec 1977. 17
- [118] A. Voros, “Semi-classical ergodicity of quantum eigenstates in the wigner representation,” in *Stochastic Behavior in Classical and Quantum Hamiltonian Systems* (G. Casati and J. Ford, eds.), (Berlin, Heidelberg), pp. 326–333, Springer Berlin Heidelberg, 1979.
- [119] M. V. Berry, “Semiclassical mechanics of regular and irregular motion,” *Les Houches lecture series*, vol. 36, pp. 171–271, 1983. 17
- [120] G. Casati, F. Valz-Gris, and I. Guarneri, “On the connection between quantization of nonintegrable systems and statistical theory of spectra,” *Lettere al Nuovo Cimento (1971-1985)*, vol. 28, pp. 279–282, 1980. 17
- [121] F. Haake, S. Gnutzmann, and M. Kuš, *Level Repulsion*, pp. 71–84. Cham: Springer International Publishing, 2018. 18
- [122] Z. Rudnick, “What is quantum chaos,” *Notices of the AMS*, vol. 55, no. 1, pp. 32–34, 2008. 18
- [123] P. Bourgade and J. P. Keating, *Quantum Chaos, Random Matrix Theory, and the Riemann  $\zeta$ -function*, pp. 125–168. Basel: Springer Basel, 2013. 18
- [124] M. V. Berry, M. Tabor, and J. M. Ziman, “Level clustering in the regular spectrum,” *Proceedings of the Royal Society of London. A. Mathematical and Physical Sciences*, vol. 356, no. 1686, pp. 375–394, 1977. 18
- [125] M. V. Berry, M. Tabor, and J. M. Ziman, “Level clustering in the regular spectrum,” *Proceedings of the Royal Society of London. A. Mathematical and Physical Sciences*, vol. 356, no. 1686, pp. 375–394, 1977. 18
- [126] M. Mehta, *Random Matrices*. Pure and Applied Mathematics, Academic Press, 2004. 18
- [127] F. Haake, *Random-Matrix Theory*, pp. 61–143. Berlin, Heidelberg: Springer Berlin Heidelberg, 2010. 18
- [128] Y. Y. Atas, E. Bogomolny, O. Giraud, and G. Roux, “Distribution of the ratio of consecutive level spacings in random matrix ensembles,” *Phys. Rev. Lett.*, vol. 110, p. 084101, Feb 2013. 18, 19
- [129] N. Chavda, “Distribution of level spacing ratios using one-plus two-body random matrix ensembles,” *Pramana*, vol. 84, pp. 309–316, 2015. 19
- [130] O. Giraud, N. Macé, E. Vernier, and F. Alet, “Probing symmetries of quantum many-body systems through gap ratio statistics,” *Phys. Rev. X*, vol. 12, p. 011006, Jan 2022. 18
- [131] V. Oganesyan and D. A. Huse, “Localization of interacting fermions at high temperature,” *Phys. Rev. B*, vol. 75, p. 155111, Apr 2007. 18
- [132] L. Susskind, “Entanglement is not enough,” *Fortschritte der Physik*, vol. 64, no. 1, pp. 49–71, 2016. 19
- [133] L. Susskind, “Computational complexity and black hole horizons,” *Fortschritte der Physik*, vol. 64, no. 1, pp. 24–43, 2016. 19
- [134] J. Eisert, M. Cramer, and M. B. Plenio, “Colloquium: Area laws for the entanglement entropy,” *Rev. Mod. Phys.*, vol. 82, pp. 277–306, Feb 2010. 19
- [135] L. V. Iliesiu, M. Mezei, and G. Sárosi, “The volume of the black hole interior at late times,” *Journal of High Energy Physics*, vol. 2022, no. 7, pp. 1–37, 2022. 19
- [136] L. V. Iliesiu, M. Mezei, and G. Sárosi, “The volume of the black hole interior at late times,” *Journal of High Energy Physics*, vol. 2022, p. 73, Jul 2022. 19
- [137] H. A. Camargo, V. Jahnke, H.-S. Jeong, K.-Y. Kim, and M. Nishida, “Spectral and krylov complexity in billiard systems,” *Phys. Rev. D*, vol. 109, p. 046017, Feb 2024. 19, 20
- [138] V. Balasubramanian, R. N. Das, J. Erdmenger, and Z.-Y. Xian, “Chaos and integrability in triangular billiards,” 2024. 20
- [139] H. A. Camargo, K.-B. Huh, V. Jahnke, H.-S. Jeong, K.-Y. Kim, and M. Nishida, “Spread and spectral complexity in quantum spin chains: from integrability to chaos,” *Journal of High Energy Physics*, vol. 2024, p. 241, Aug 2024. 19, 20
- [140] J. Erdmenger, S.-K. Jian, and Z.-Y. Xian, “Universal chaotic dynamics from krylov space,” *Journal of High Energy Physics*, vol. 2023, no. 8, pp. 1–62, 2023. 20
- [141] A. Aleman, A. Montes-Rodríguez, and A. Sarafoleanu, “The eigenfunctions of the hilbert matrix,” *Constructive Approximation*, vol. 36, pp. 353–374, Dec 2012. 20
- [142] E.-M. Graefe, “Quantum chaos on display,” *Physics*, vol. 6, p. 9, 2013. 22
- [143] P. Richens and M. Berry, “Pseudointegrable systems in classical and quantum mechanics,” *Physica D: Nonlinear Phenomena*, vol. 2, no. 3, pp. 495–512, 1981. 22
- [144] A. Bäcker, F. Steiner, and P. Stifter, “Spectral statistics in the quantized cardioid billiard,” *Phys. Rev. E*, vol. 52, pp. 2463–2472, Sep 1995. 22
- [145] H. P. Baltes and E. R. Hilf, “Spectra of finite systems: a review of weyl’s problem, the eigenvalue distribution of the wave equation for finite domains and its applications on the physics of small systems,” (*No Title*), 1976. 22
- [146] A. Bäcker, S. Fürstberger, R. Schubert, and F. Steiner, “Behaviour of boundary functions for quantum billiards,” *Journal of Physics A: Mathematical and General*, vol. 35, no. 48, p. 10293, 2002.
- [147] W. Müller, “Weyl’s law in the theory of automorphic forms,” *arXiv preprint arXiv:0710.2319*, 2007. 22
- [148] A. Parretta and G. Calabrese, “About the definition of ‘multiplier’of an integrating sphere,” *Int. J. Opt. Appl.*, vol. 3, no. 6, pp. 119–124, 2013. 24
- [149] R. D. Luca, “The path of a light ray in a semicircular cavity,” *Physics Education*, vol. 58, p. 065018, sep 2023. 24

## Appendix A: Visualisation of quantum scars

### 1. The probability density distributions for Circular and Oval billiards

In Fig. (15) represents the probability density distributions for a few selected eigenstates of circular and oval billiards. Within these integrable billiard systems, regions of high probability density concentrate along caustics generated by classical periodic trajectories. In circular billiard, these high density eigenstates mainly exhibit three types of shapes; straight-line bouncing paths, petal-like structures and concentric nodal rings as shown in Fig. (15(a)). While in the oval boundary, these regions align along confocal ellipses and hyperbolic caustics, shown in Fig. (15(b)).

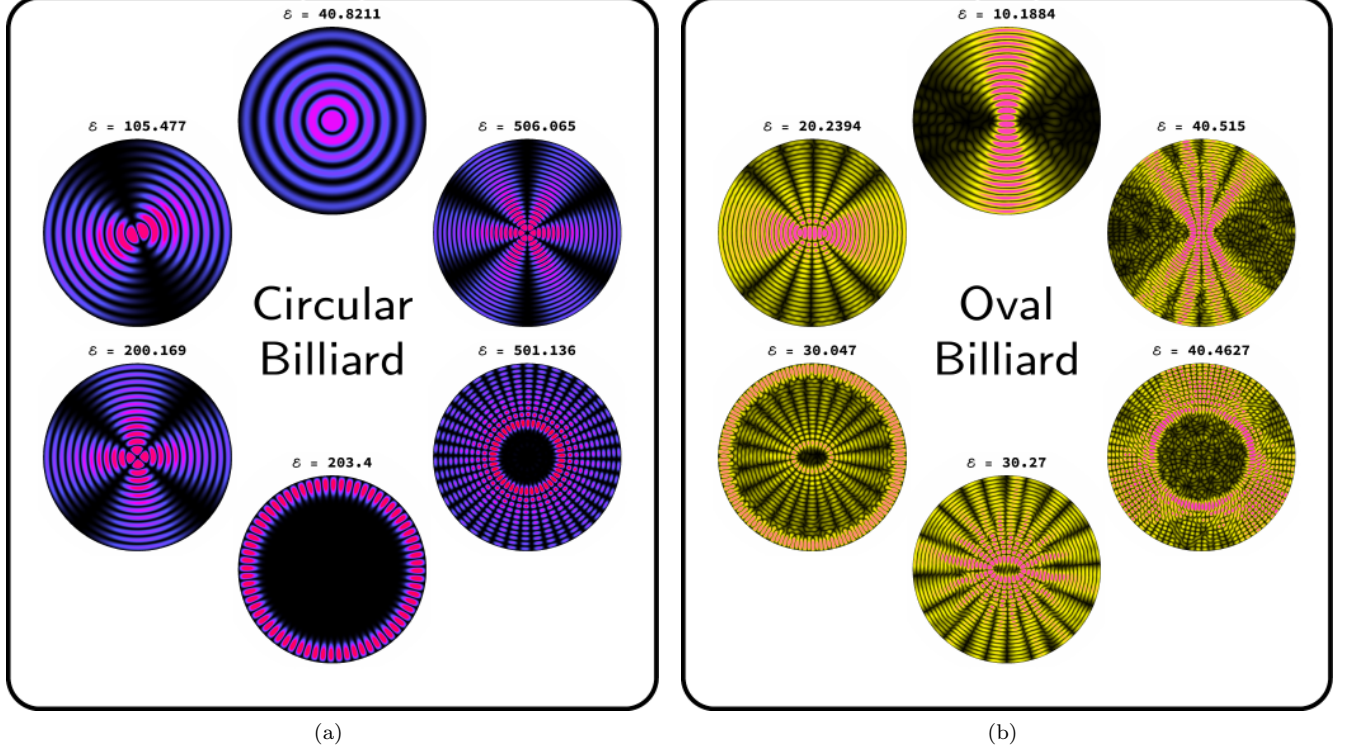
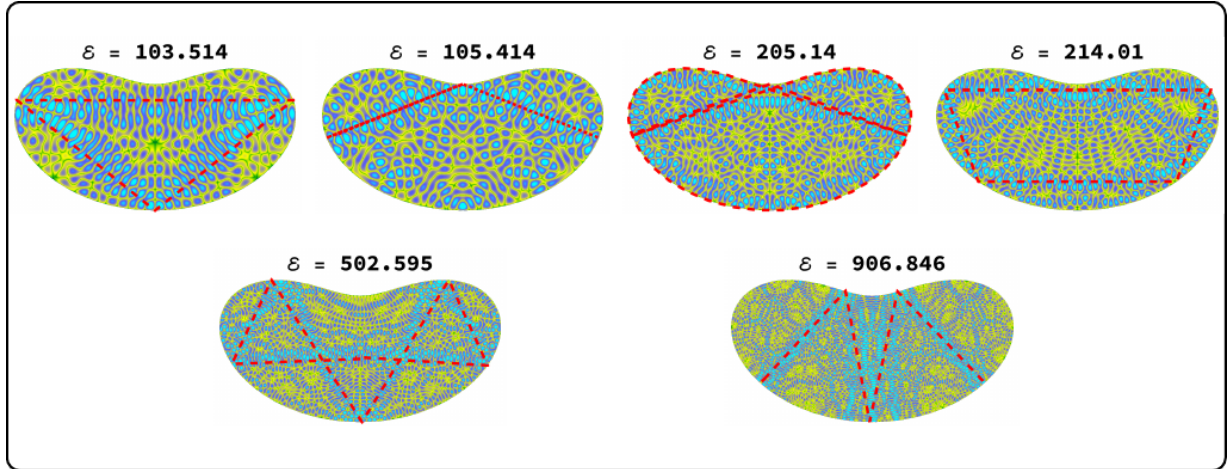


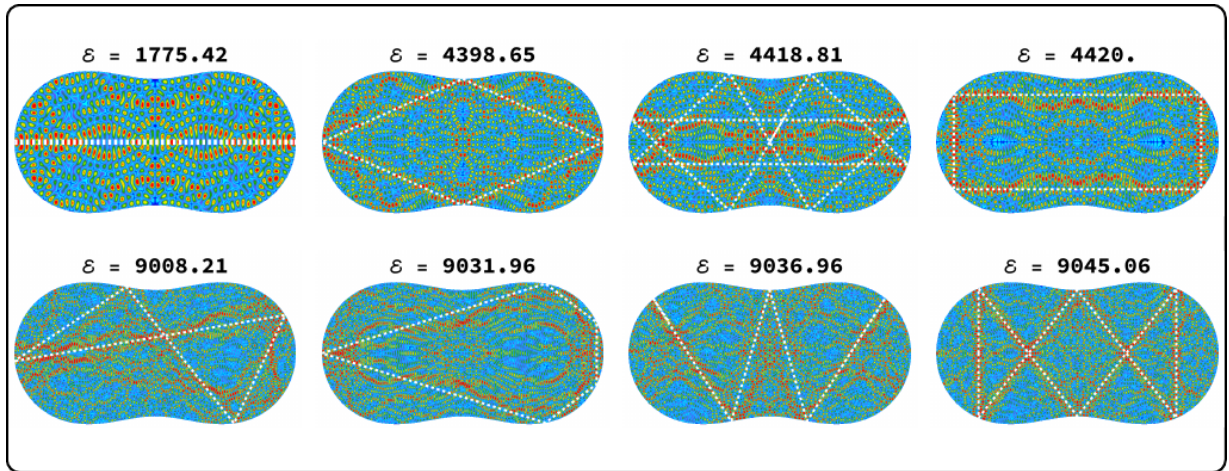
FIG. 15. The probability density distributions for eigenstates are displayed for billiards: (a) circular billiard, (b) oval billiard. In these integrable billiards, the local density regions are reminiscent of caustics found in corresponding classical systems.

### 2. Scars for the slow diverging trajectories

In Fig. (16), probability densities of some of these eigenstates. These eigenstates are subtlety scarred by the slow diverging trajectories, and thus weakly breaking the ergodicity. These initially formed, high-density regions persist, remaining visible indefinitely.



(a)



(b)

FIG. 16. Quantum scars for slow diverging trajectories in (a) bean billiard and (b) peanut-shaped billiard. The red and white dashed line represent slow diverging trajectories.